Supplementary Materials and Methods

Genes

Sequences for voltage (PROPS), calcium (GCaMP6f), pH sensors (super-ecliptic pHluorin), and mRuby3 were all taken from previously published papers. PROPS was a gift from Adam Cohen (pJMK001 – addgene plasmid 33780), GCaMP6f was a gift from Douglas Kim (pGP-CMV-GCaMP6f – addgene plasmid 40755), pKanCMV-mClover3-mRuby3 was a gift from Michael Lin (Addgene plasmid # 74252), and super-ecliptic pHluorin was constructed as a gBlock (IDT) using the IDT *E. coli* codon optimized sequence. CaPR was constructed by fusing PROPS and GCaMP6f while maintaining the His-tag linker at the end of PROPS. Constitutive GCaMP6f was constructed by fusing GCaMP6f to mRuby3. mRuby3 was included to ensure that all cells were quantified when manipulating calcium levels. Both constitutive CaPR and GCaMP6f construction was carried out initially in the pBAD plasmid using isothermal cloning, then moved to the constitutive backbone described below. A second construct using separate ORFs was generated using the petDUET expression plasmid. Sequences for new constructs are provided in the supplementary text.

Expression of the sensors was accomplished using the pBAD (arabinose inducible), petDUET (IPTG inducible) or 118 (sigma 70 constitutive) backbones. The pBAD plasmid was obtained from Addgene (#33780) and the petDUET backbone was purchased from EMDMillipore (71146-3). The constitutive expression vector was assembled using a combination of biobricks part BBa_J61002 (derived from pSB1A2), part BBa_J23118, and pBAD. The BBa_J61002/BBa_J23118 plasmid was digested using Pst1 and Spe1 to remove the protein generating part downstream of the constitutive 118 promoter. Genes of interested (GOI) were then amplified from the pBAD plasmid containing the GOI as to include the upstream RBS (T7) and downstream terminator (rrnB terminator). Amplicons were then assembled into the digested backbone using Gibson assembly reconstituting a protein generating part containing the GOI.

Expression conditions varied for each plasmid. For pBAD, cells from an overnight culture were diluted 1:100 and grown to an OD of ~0.4. Arabinose was added to a final concentration of .0005% and cells were incubated for 3-5 hours at 37 °C. If PROPS was included, a final concentration of 5 μM retinal was added at the same time as arabinose. Cells were taken directly from the LB and placed on agarose pads or PLL coated plates for imaging. The PLL adhered cells were left to adhere for an hour, followed by extensive washing with the M9 minimal medium to remove non-adhered cells. Expression in the petDUET occurred similarly, except 0.5 μM IPTG was added in place of arabinose. Plasmids containing the 118 promoter are constitutively expressed, and 5 μM retinal was added to the overnight culture as well as the diluent.

All new plasmids from this study have been deposited with and are distributed through Addgene. These include the constitutive CaPR (pKL001, Addgene plasmid no. 98917), petDUET inducible CaPR (pKL002, Addgene plasmid no. 98921), constitutive PROPS (pKL003, Addgene plasmid no. 98919), and constitutive GCaMP6f-mRuby3 (pKL004, Addgene plasmid no. 98920).

Strains

All experiments used the BW25113 background as the parent strain except when using the petDUET plasmid, which used BL21 *E. coli*. Glycerol stocks were maintained at -80 °C, and individual colonies were picked for each experiment. Cells were grown in LB with their expression plasmid's respective antibiotic selection added at 37 °C with shaking. OD measurements were taken on an Ocean Optics Flame miniature spectrometer.

Imaging

Imaging took place either in a Nikon NSTORM microscope equipped with a TIRF module or with a custom, widefield inverted microscope.

Nikon NSTORM – We used a Nikon NSTORM microscope with a 100x 1.45 NA objective using laser excitation imaged onto an Andor 897 EMCCD. All measurements were conducted with a high illumination angle to maximize signal to noise ratio. For PROPS illumination, a 561 nm laser at 14 W/cm^2 intensity with 200 ms exposure time was used. A quadband filter (405/488/561/637) with a laser blocking filter was used for imaging PROPS. GCaMP6f fluorescence was excited with a 488 nm laser at 1200 mW/cm^2 intensity for the CaPR construct and 620 mW/cm^2 intensity for GCaMP6f alone with 200 ms exposure time using the same quadband dichroic. Dual illumination of CaPR occurred using a 2 camera setup. Excitation was reflected by the quadband cube with 488 and 561 nm lasers simultaneously exciting the cells. A 561 nm dichroic split the emission light. A 525/50 nm emission filter was used for the GCaMP signal, while a 700/75 emission filter was used for PROPS. Typical exposure times for CaPR measurements were 200 ms with a 300x EM gain. Imaging of the CaPR construct did not exceed 3 minutes of total light exposure time in any reported experiments.

Custom microscope – We also used a custom, homebuilt microscope to image CaPR expressing cells. A 60x Olympus TIRF lens (NA 1.45) was imaged onto an Andor 888 Ultra EMCCD. Coherent OBIS lasers at 488 nm (488 LX 150 mW) and 561 nm (561 LS 50 mW) simultaneously illuminated the sample. The emission light was reimaged through a dichroic splitter to image the GCaMP6f and PROPS fluorescence on opposing halves of the camera. Emission filters used were a 520/30 and a 580LP, respectively. Typical exposure settings were 200 ms with a 300x EM gain. The microscope was controlled using custom Labview (National Instruments) scripts.

Imaging media compositions

Minimal media was made to a final concentration of 1X M9 salts (Sigma) with 0.4% w/v glucose then adjusted to a pH of 7.5 with sodium hydroxide. In the case of experiments occurring at pH other than 7.5, HEPES was added to a final concentration of 5mM and pH was adjusted as indicated. In the case of experiments occurring at different osmolality, sorbitol was added to the final concentration indicated.

Supplemented minimal medium was made in the same fashion as minimal medium above with the following additions to the final concentrations of: 2mM magnesium sulfate, 100µM calcium chloride, 1X Gibco MEM vitamin solution, and 1X Gibco MEM amino acid solution (ThermoFisher).

Phosphate free media was made to a final concentration of 1.752 g/L sodium chloride, 1.125 g/L potassium chloride, and 0.525 g/L ammonium chloride with 0.4% w/v glucose then adjusted to a pH of 7.5 with sodium hydroxide. In the case of experiments utilizing phosphate free media with calcium, calcium chloride was added to a final concentration of 5mM.

Imaging conditions

All cells were imaged within 1 hour of specified treatment unless otherwise noted

Agarose pads – For 1% agarose pads, low-melt agarose was added to a given media above to a final concentration of 1% w/v then heated until the agarose dissolved. Once in solution, the mixture was cooled

in silicone molds and pads were cut from the agarose media gels. Unless otherwise noted, cells were placed directly on pads and imaged. In the case of nifedipine, verapamil, and CCCP compounds were added to their final indicated concentration to 37˚C liquefied agarose minimal media pH 7.5, then cooled and cut into pads.

PLL adhesion – A 0.001% w/v solution of PLL was dried on glass. Cells were then adhered for 1 hour in LB then washed 3 times in the medium in which they were to be imaged. When comparing the adhered and pad conditions, the final wash in the pad condition was replaced by the addition of an agarose pad made with minimal medium on top of the adhered cells. PLL coated glass was always prepared the same day.

Gelatin pads – A 10% w/v solution of gelatin in minimal medium was made and placed at 4˚C for 4 hours, then warmed to 25˚C before imaging.

Other chemical adherents – A 0.5 mg/ml solution of concanavilin, or 0.1 mg/ml solution of polyethylenimine was dried on glass. Cells were then adhered and washed in the same fashion as in the PLL adhesion protocol.

Mechanical pressure

Measurements of the same PLL adhered cells before and after contact with an agarose pad were taken on the NSTORM microscope equipped with a perfect-focus system. An agarose pad was gelled onto the end of a pipet tip and mounted onto a PT3 translation stage (Thorlabs). Imaging started with the cells immersed in minimal medium, and the pad was lowered onto the sample using the PT3 stage. As soon as focus was transiently changed < 10 μm from the starting focal point, movement was stopped and the perfect-focus recovered.

YFP fusion lines

To measure single cell, *in vivo* protein concentration, we imaged cells expressing a YFP tag fused to the endogenous gene (1). Strains were acquired from the *E. coli* Genetic Stock Center at Yale University via a transfer agreement from Harvard University. Cells were grown using the same method as PROPS expression excepting chloramphenicol was used for selection. Bacteria were immobilized using PLL in a 96-well glass bottom plate (Mattek) and were subsequently washed three times in an equal volume of minimal media. To each strain after washing, either liquid (minimal medium) or a pad (1% agarose in minimal medium) was added. Cells were then imaged once an hour for each hour on the NSTORM microscope. The Elements tiling software was used to generate a 12 x 3 image (974 x 244 μm). Each strain was imaged at 3 laser powers, 2.9, 8.2, 20.2 W/cm^2 for a 200 ms exposure at 300x EM gain, and the highest intensity without saturating was used for the analysis.

To analyze the YFP strains, a laser illumination pattern was generated by averaging together each strain under each condition and using a Gaussian blur (35 x 35 pixels). Each image was then divided by the illumination pattern, and a tophat filter was used to eliminate background. Cells were then segmented by a marker controlled watershed and the mean intensity for each cell was calculated. The population of cells was then plotted as a histogram fit to Gaussian distributions.

Knockouts

Single knockouts measured were obtained from the Keio collection (2). The entire collection, assembled in duplicate, was obtained from Dharmacon (#OEC4988). The MSC triple knockout (MJF465, ΔmscS, ΔmscL, ΔkefA) was a gift from Rob Phillips. Each strain carries a non-essential gene replaced with a kanamycin resistance cassette. These strains were then transformed with the constitutively expressing CaPR plasmid. Initial transformants were grown on agarose plates containing kanaymycin and ampicillin to ensure both the plasmid and resistance cassette were still present. For imaging, cells were grown overnight only in the presence of ampicillin to remove bias from translation inhibition by kanamycin. Knockout strains were grown overnight in a 96 well plate in the presence of 5 μM retinal. Cells were then adhered to the bottom of a 96 well PLL-coated glass bottom plate for one hour and washed three times in M9 minimal media. In each well following the wash step, an agarose pad was placed on top of the adhered cells, and the cells were imaged in serial on the NSTORM.

Flow cell

Flow cells were constructed from 2 mm thick silicone, cut to form a channel. The silicone channel was pressed between a coverslip which was used to adhere bacteria, and a glass slide with two holes drilled 15 mm apart and 18 gauge needles adhered. Media flowed through this chamber at a rate of 100 μl/s. To control the oscillating media conditions, an Arduino (Arduino One) controlling two solenoid pinch valves alternated between 50 s closed, 10 s open state in order to flow media through 1/32" ID Tygon Tubing from the reservoir into the flow cell chamber. Experiments had conditions that alternated every 30 s for up to 4 hours.

pHluorin pH titration

PROPS and super ecliptic pHluorin were expressed together on the petDUET plasmid which contains two distinct ORFs. Cells containing the dual plasmid were grown overnight in LB and diluted 1:100 in fresh medium, and grown to an OD of 0.1 at 600 nm. IPTG was added to induce the cells for 3 hours at a concentration of 500 μM. These cells were placed into a flow chamber as described above and adhered with PLL. CCCP at a concentration of 20 μM was added to the cells to set the internal pH equal to the external pH, and was present in all pH buffers added afterwards. Medium of varying pH was added to the cells and the mean fluorescence was recorded. Each individual cell was fit to a hill curve. From each cell, the pKa binned in a histogram and fit to a normal distribution. The peak of the normal distribution was identified as the pKa with a value of 7.6.

Computer code

All analysis was performed using custom scripts written in Matlab R2016b (Mathworks, Inc). Scripts and all data sets are available to researchers upon request.

Trace extraction:

Movies from a given day were first averaged together to form an illumination profile using a Gaussian blur of 35 x 35 pixels. Then each movie was again individually loaded for segmentation and time trace extraction. Movies were first aligned using an automatic image registration every 10 frames and interpolated linearly between the registered frames. Next the illumination was divided from every frame to yield a flatter intensity profile. The background was subtracted using a tophat morphological operator preceded by a 3 x 3 median filter. The structured element used was a ball of radius 50 pixels. The movie was then averaged across all the frames to segment individual cells. Segmentation used a modified marker

controlled watershed algorithm to identify individual cells. A dilation of the image was created using a square sized 2 x 2 and that image was subtracted from the original to outline individual cells. After a thresholding and a dilation of the outline, the basins were used as the markers for the watershed algorithm. The watershed.m command in Matlab was used for this portion. Time traces were then calculated using the mean intensity of each ROI at every time point.

Voltage peak detection:

The peak detection for voltage is described in greater detail in the supplementary text at the end of this appendix.

Briefly, finding peaks in the voltage data is accomplished through a sequence of classification and clustering algorithms. The time series is normalized by dividing by the standard deviation of the data and is classified into four categories by considering clusters of points in the Poincare plot (map) of the time series. For a time-series given by a sequence of values given by $y(t)=\{x(t_1),x(t_2),x(t_3),\ldots x(t_n)\}$ the Poincare map is formed by plotting ordered pairs of points $(x(t_{n-1}),x(t_n))$. A 2-D histogram is calculated using the Poincare map by binning the data $(x(t_{n-1}),x(t_n))$ over a uniform 2-D grid. Approximate local densities are found by dividing the counts in the histogram of the Poincare map by the total number of data points in the Poincare map. The density is re-scaled onto the interval [0, 1]. Finding the data in the Poincare map above a sequence of density thresholds, specifically, 0 and 0.1 forms hierarchical clusters. The time-series is classified into one of four categories by considering the convex hull of the density clusters. Specifically, if the centroid of the lowest threshold convex hull (0) is outside the convex hull of the higher threshold cluster (0.1), indicates a time-series includes excursions from central mean value. The case where the centroid of the lowest threshold convex hull (0) is inside the convex hull of the higher threshold cluster (0.1) indicates the excursions from a mean value in the time-series is distributed throughout the domain of the time-series such as bi-modal data, i.e. where the data shifts from variations around a mean value to variations around a different mean value, small variations superimposed on a slowly varying trend, and data that has numerous peaks throughout the domain of the time-series. Calculating the R-square of the data inside the convex hull and considering if the centroid of the low threshold convex hull falls in a low-density region of the high threshold convex hull can resolve the final three categories (bi-modal, trend, peaks). Sequences of points in the time-series above a threshold value are found where the threshold used is the 55^{th} percentile of the data points inside the higher threshold cluster in delay space. Statistics are calculated using only the time series classified as containing peaks.

Calcium peak detection:

Calcium peaks were detected by first removing the baseline through an erosion function across 20 seconds, followed by a wavelet denoising using the default values returned by the Matlab function ddencmp.m. The differential of the denoised trace was used to identify positive and negative going slopes. To be flagged as a peak start, the area under the curve of the difference trace had to be at least 3.5x larger than the standard deviation of the entire trace. After flagging a peak start, the end of the peak was defined either by the start of a new peak or a negative area under the curve meeting the same criteria as above, whichever came first. The start and stop time were called as the maximum slope, and the area under the curve for each peak was calculated using the trapezoidal rule on the original time trace.

Granger causality:

Granger causality was tested using the Multivariate Granger causality toolbox (MVGC) written in Matlab(3). CaPR data was recorded and extracted using the above methods. Each cell traces were then used as input into the MVGC where each cell was considered a separate trial, with each frame considered an observation. The rest of the variables were set using the default settings in the toolbox.

Supplementary Figures:

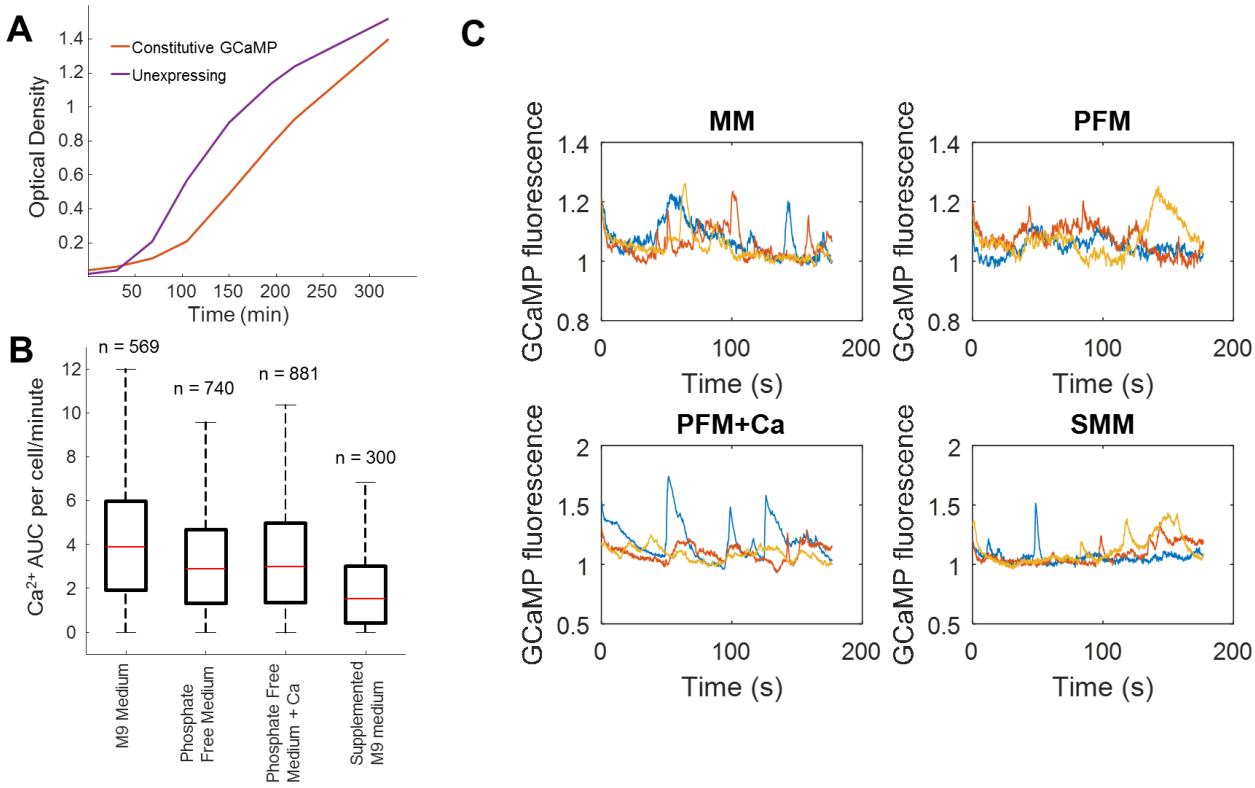

Supplementary Figure 1 – GCaMP6f expression and transients. (A) Growth curve for cells expressing GCaMP6f vs no exogenous proteins. The GCaMP6f cells grow slower likely due to cost of expressing the fluorescent protein. (B) Box plots showing calcium transients under agarose pads of a variety of different media including M9 salts with glucose, phosphate free minimal medium, phosphate free minimal medium with external calcium, and supplemented M9 minimal medium. The pH was 7.5 for all experiments. Red line indicates median, black box indicates 75/25%, and black dashed lines indicate 90/10% of the maxima. Outliers were analyzed but not shown. (C) Example fluorescence time traces from each medium condition. All cells were imaged within 1 hour of addition to an agarose pad. The Y axis is the GCaMP fluorescence normalized to the 5th percentile of each cell during the movie. Each color is a single cell from the population.

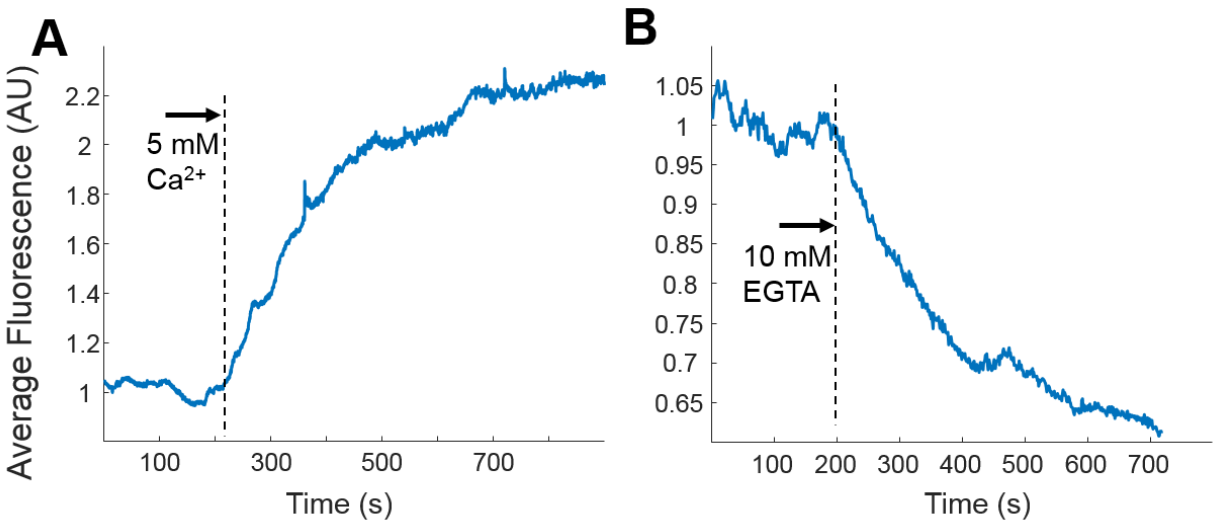

Supplementary Figure 2 – Cytoplasmic calcium responds to external calcium levels. (A) Increase in mean population of cells constitutively expressing GCaMP6f fluorescence upon addition of 5 mM external calcium. (B) Decrease in mean population GCaMP6f fluorescence after addition of 10 mM EGTA. For each condition, the Y axis is the GCaMP fluorescence normalized to the 5th percentile of the pre-treatment fluorescence trace. Calcium and EDTA were added to the top of the agarose pad at 50X concentration.

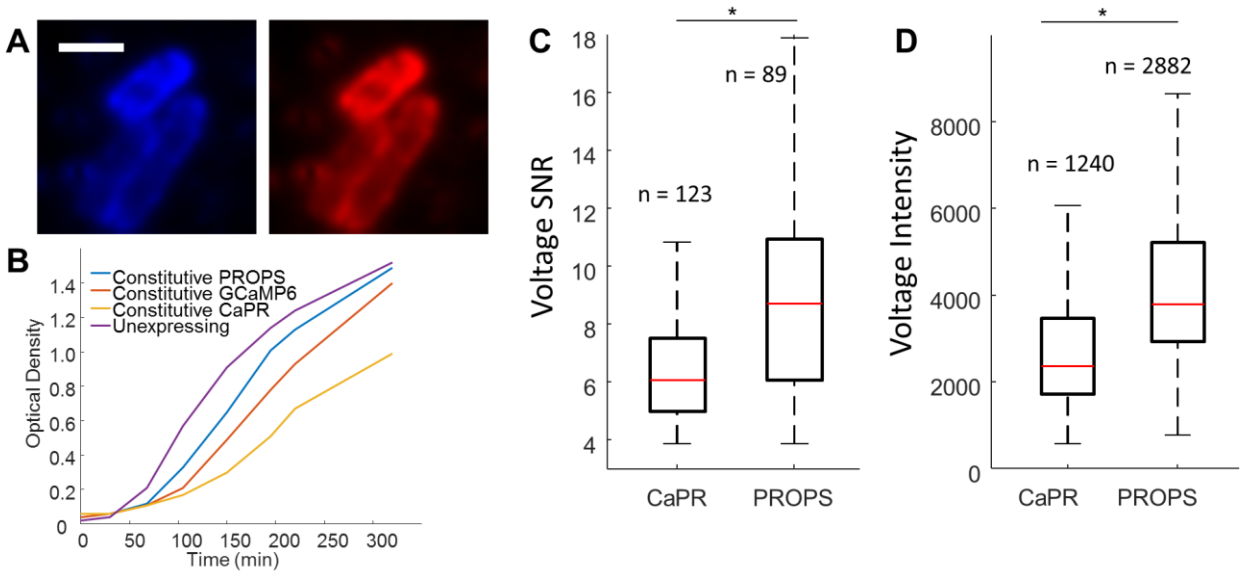

Supplementary Figure 3 – CaPR is membrane localized, slows growth and has lower SNR than PROPS alone. (A) Image of *E. coli* constitutively expressing CaPR–PROPS (right, false colored red) fused to GCaMP6f (left, false colored blue)–imaged under an agarose pad. Scale bar is 2 µm. (B) Optical density measured at 600 nm over time shows the growth curve for cells constitutively expressing PROPS (blue), GCaMP6f fused to mRuby3 (red), and CaPR (yellow), vs no exogenous proteins (purple). (C) Signal to noise ratio of voltage peaks calculated in the fused CaPR construct or in the PROPS alone construct. The mean SNR is 43% higher in cells expressing PROPS alone. (D) Average fluorescence intensity in cells after CCCP addition expressing fused CaPR or PROPS alone. The average intensity in PROPS alone cells was 60% higher than in the fused CaPR construct. (C & D) Red line indicates median, black box indicates 75/25%, and black dashed lines indicate 90/10% of the maxima. Outliers were analyzed but not shown. * represents a p value < .001 in an unpaired t-test with unequal variance.

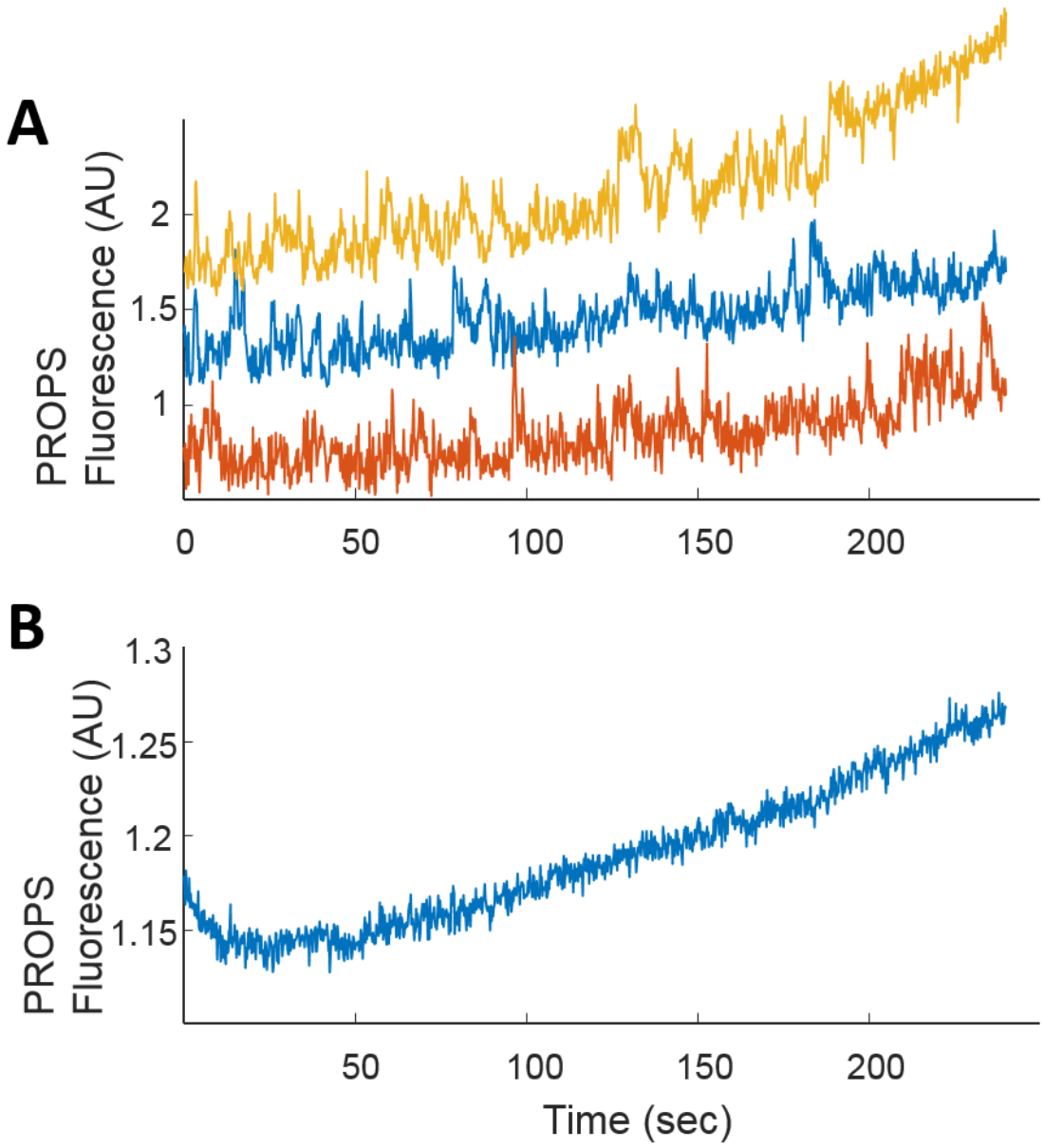

Supplementary Figure 4 – Phototoxicity in PROPS expressing cells. (A) Example traces from single cells of PROPS measurements during excitation with 561 nm and 488 nm lasers. Cells were seen to depolarize as indicated by an increase in fluorescence over time. (B) Population average of cells expressing CaPR during excessive illumination conditions. To avoid potential artifacts, continuous CaPR measurements were restricted to < 2 minutes.

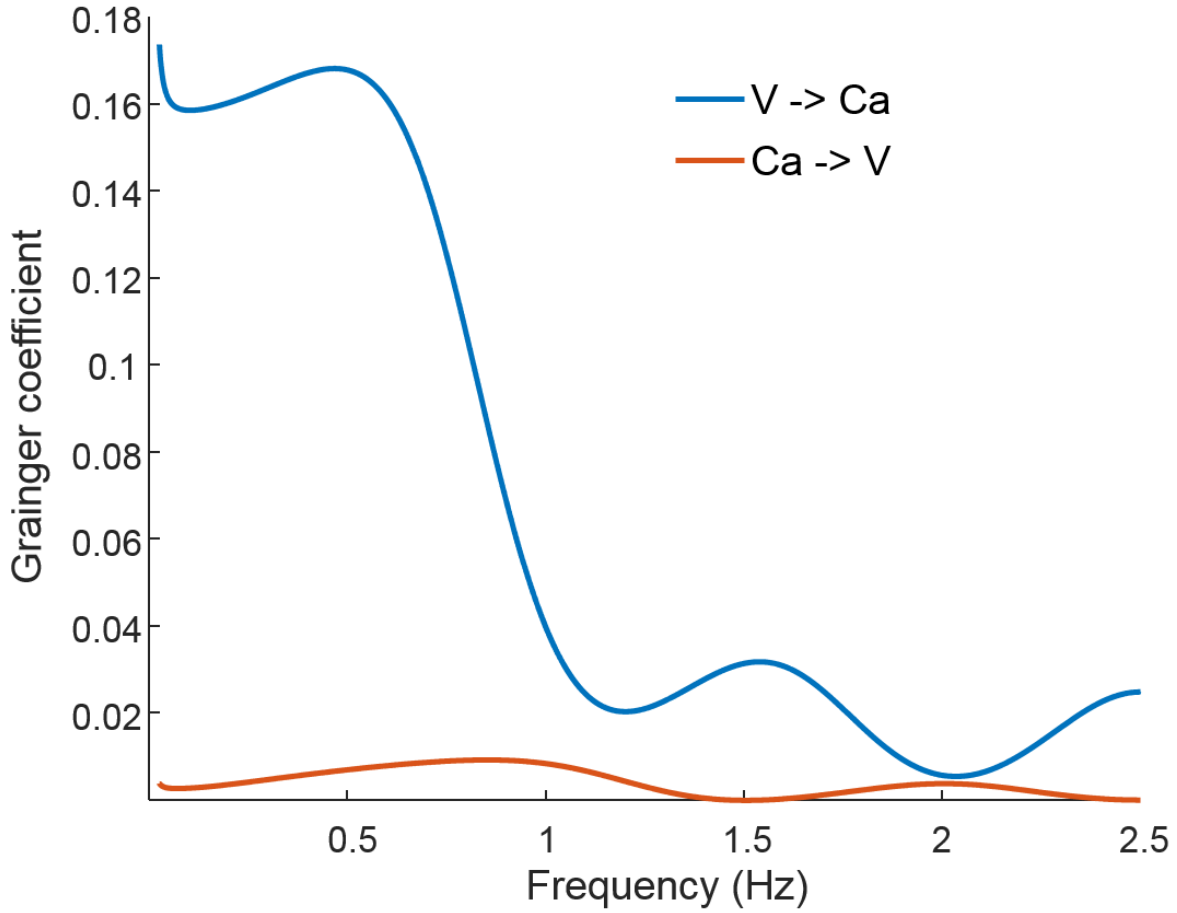

Supplementary Figure 5 – Voltage transients induce calcium influx. A Granger causality analysis predicted strong likelihood of fluctuations in voltage inducing similar changes in calcium, with little predictive power for calcium influencing voltage.

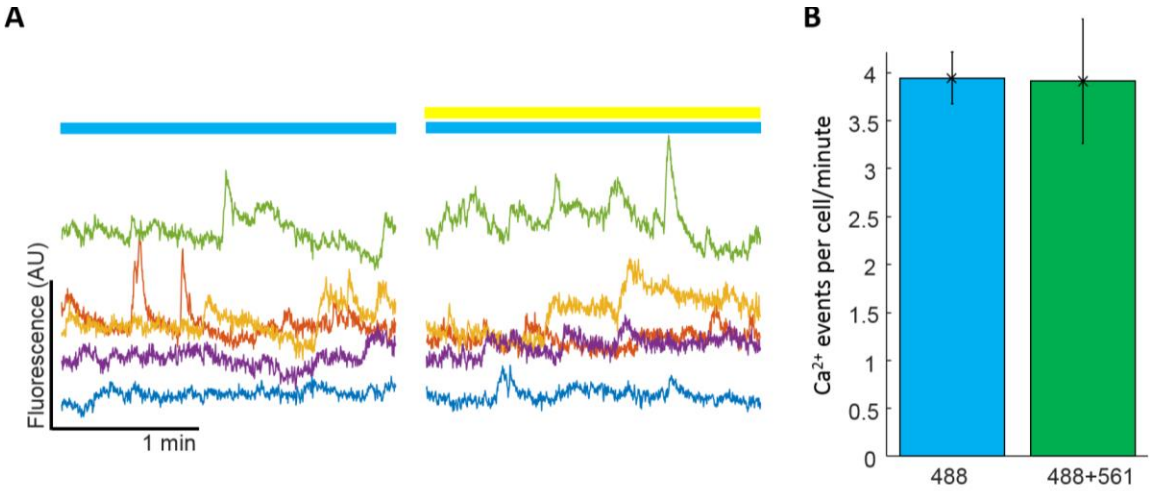

Supplementary Figure 6 – Yellow light did not affect calcium transients. (A) Cells expressing CaPR were measured before and after the presence of yellow light used to image PROPS. The number and amplitude of transients were unaffected by the yellow laser light. (B) Calculated number of calcium transients in the same cells either under 488 nm light alone, or under dual excitation with 488 and 561 nm (n = 127 cells). Error bars show the standard error of the mean.

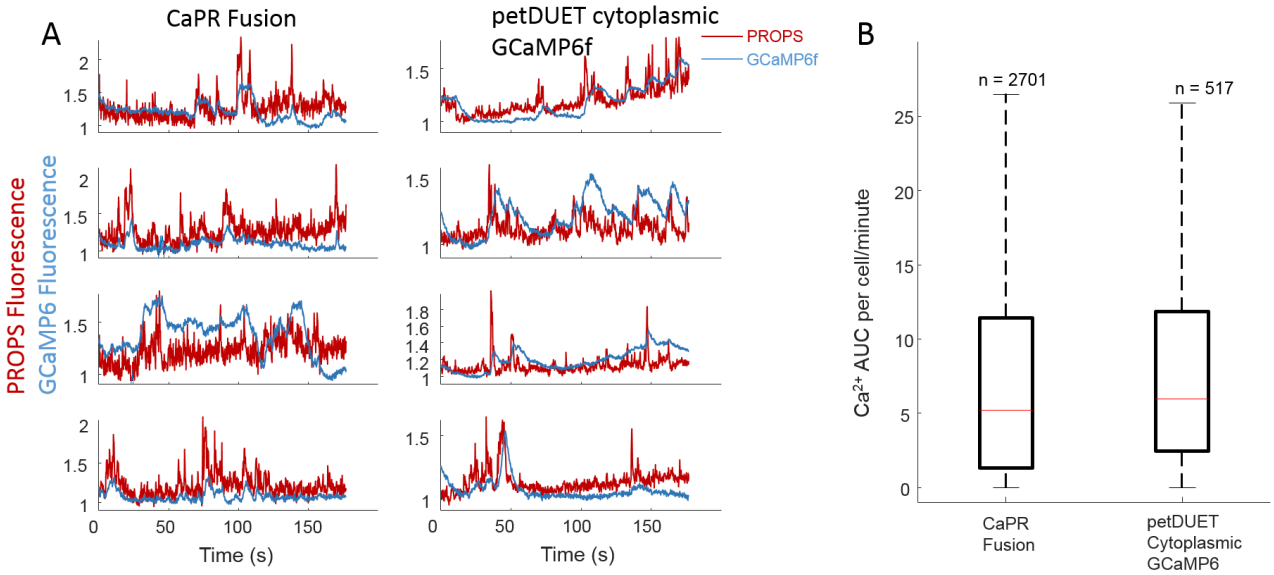

Supplementary Figure 7 – Fused and cytoplasmic GCaMP report voltage induced calcium flux. (A) Normalized single cell representative traces for the fused CaPR construct (left column) and the cytoplasmic GCaMP6f with transmembrane PROPS (right column). The red trace is PROPS and blue is GCaMP6f. (B) Calcium AUC measurements for populations of cells under an agarose pad of M9 minimal medium with glucose at pH 7.5 for both constructs. Red line indicates median, black box indicates 75/25%, and black dashed lines indicate 90/10% of the maxima. Outliers were analyzed but not shown.

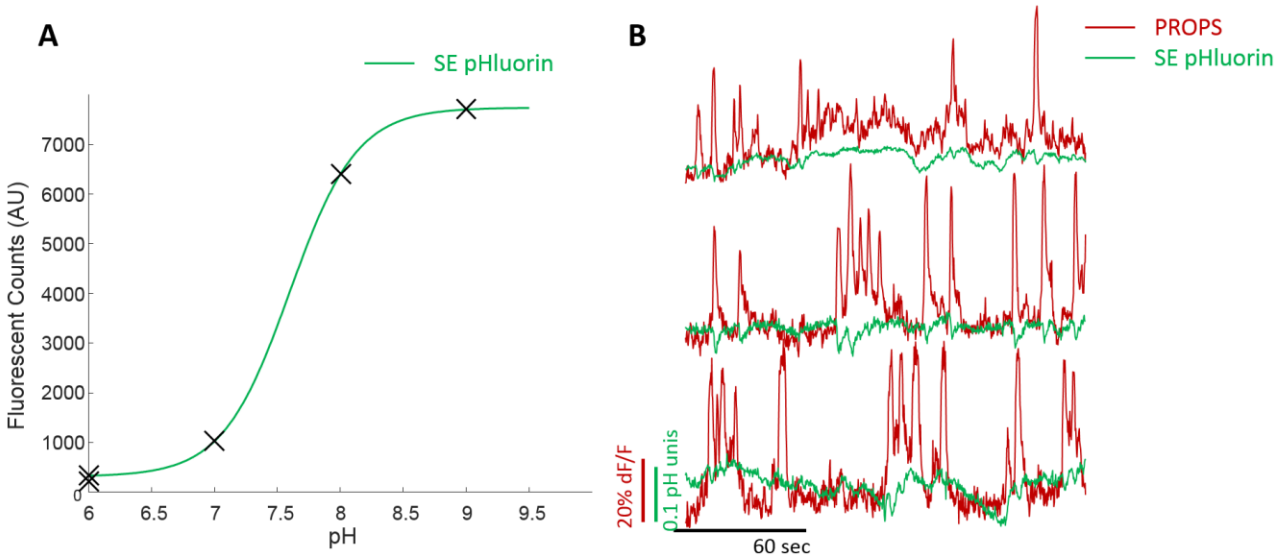

Supplementary Figure 8 – The fluorescent transients are not due to changes in pH. (A) A pH calibration curve of cells dually expressing PROPS and super ecliptic pHluorin. The curve fit to a pKa of 7.6. (B) Cells expressing PROPS and super ecliptic pHluorin were measured during voltage transients. Using the previous curve, we measured pH changes during voltage transients and found them to slightly acidify (less than 0.1 units).

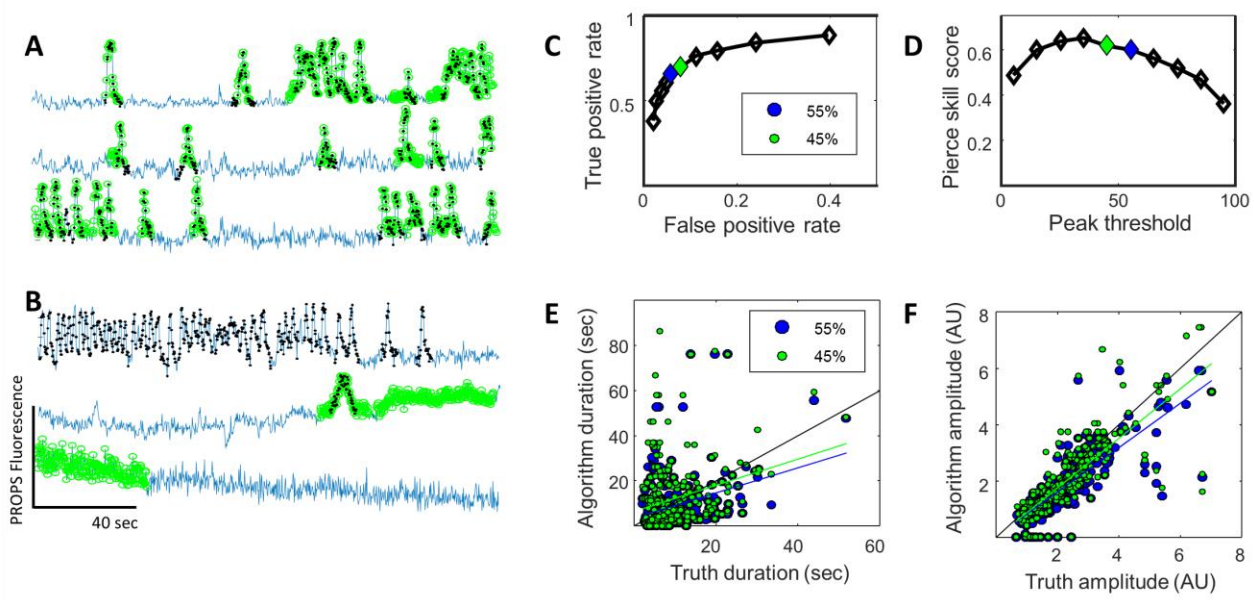

Supplementary Figure 9 – Measuring the accuracy of our automatic peak finder compared to a human-truth data set. (A) Representative traces of the peak finder identifying (green circles) peaks that were marked by manual selection (black circles). (B) Representative traces of the peak finder mis-identifying or missing voltage transients. Cases were either too noisy to identify multiple clusters, small changes be identified as large peaks, or the initial photobleaching identified as a peak. (C) Receiver operator curve comparing the automatically identified peaks to the human truth data set as a function of increasing peak threshold. Two peak thresholds at 45% (green) and 55% (blue) were chosen to pursue more closely. (D) Pierce skill score for the same peak thresholds as in the ROC curve. As the threshold increases, fewer peaks are called, but they are more accurate in identification. (E) Scatter plot comparing the duration of the peaks called by the human (x-axis) and the algorithm (y-axis). A perfect algorithm would have all points falling on the line y=x (black line). Each color represents a different value for the threshold. The algorithm does not perform well calling the duration, likely due to chaining together several concurrent transients. (F) Scatter plot comparing the amplitude of peaks called by the human (x-axis) and the algorithm (y-axis). A perfect algorithm would have all points falling on the line y=x (black line). Each color represents a different value for the threshold. The algorithm performs well calling the amplitudes of the peaks.

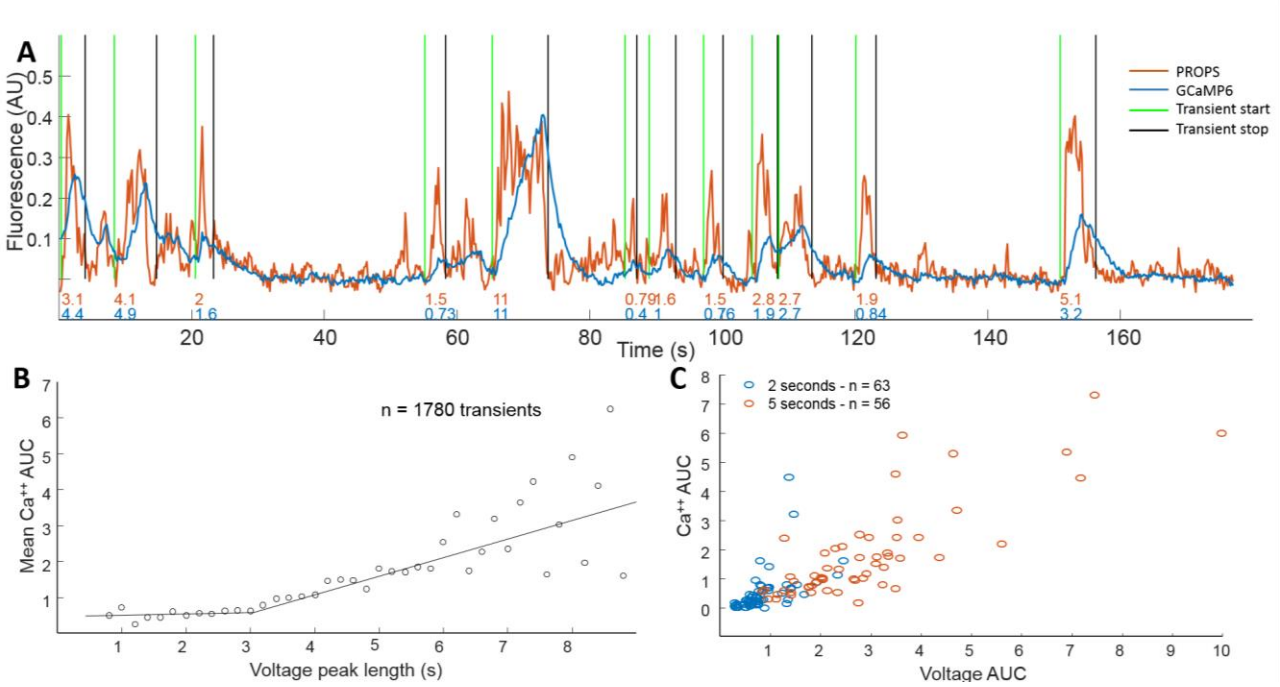

Supplementary Figure 10 – Analyzing voltage and calcium transients. (A) Representative trace of a single cell expressing CaPR and exciting both PROPS (red) and GCaMP6 (blue). Green and black lines indicate the start and stop of an identified voltage transient, respectively. The numbers represent the AUC calculated for voltage (red) and calcium (blue) for each transient. (B) Binning the voltage transients by time showed short peaks (< 3 sec) do not induce calcium. Longer peaks show a linearly increasing amount of calcium AUC with voltage duration. (C) Individual transients that were identified with 2 second duration (blue) and 5 second duration (red). Short transients have low voltage and calcium AUC, while the longer transients show a linear correlation.

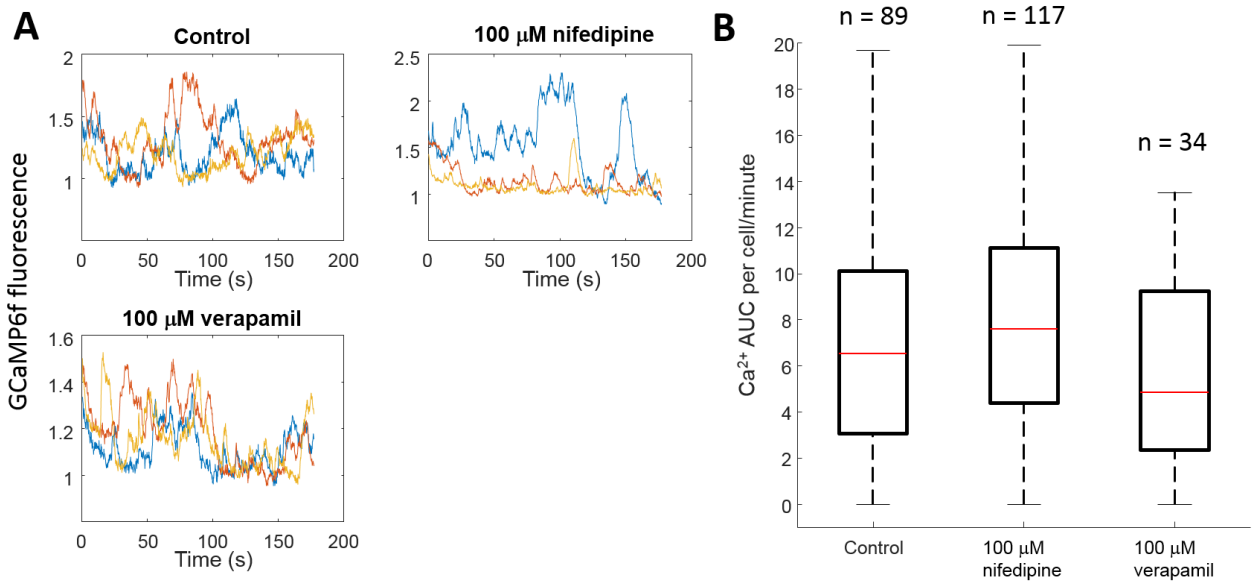

Supplementary Figure 11 – Verapamil and nifedipine do not block calcium transients. (A) Example traces showing individual cells in different colors under no treatment, 100 μM verapamil, and 100 μM nifedipine. Data were taken from cells expressing CaPR under an agarose pad at pH 7.5. (B) Box plot showing the calcium AUC for each treatment. Red line indicates median, black box indicates 75/25%, and black dashed lines indicate 90/10% of the maxima. Outliers were analyzed but not shown.

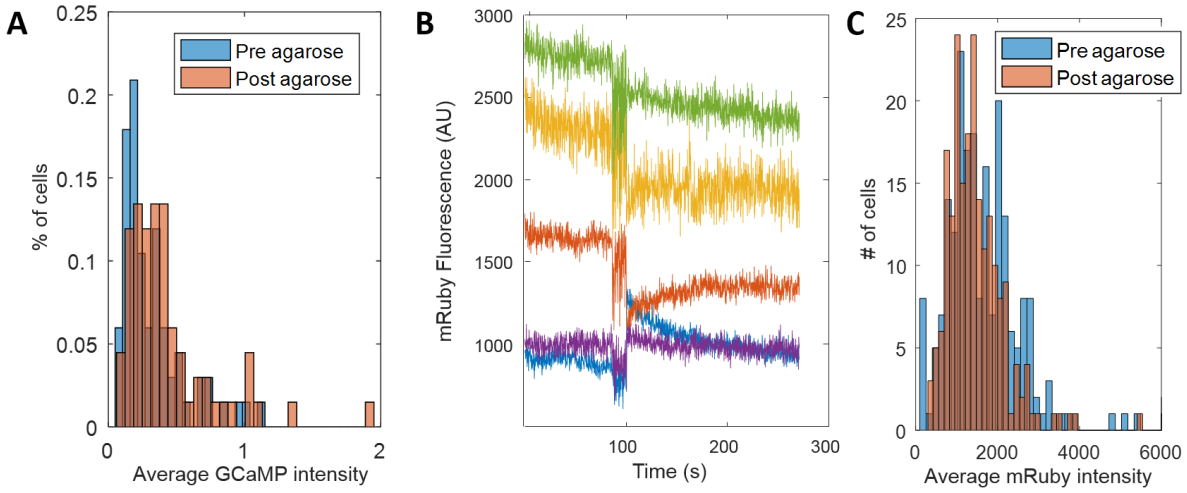

Supplementary Figure 12 – Calcium changes during mechanical stimulation are not due to optical or genetic artifacts. (A) Histogram of the boxplot data from Fig 3C showing an increase in the mean GCaMP fluorescence after addition of an agarose pad. (B) Traces of tethered mRuby3 before and after mechanical stimulation with an agarose pad. Each line represents a single cell. (C) Histogram of mRuby3 intensities before and after mechanical stimulation. The slight decrease is likely due to photobleaching.

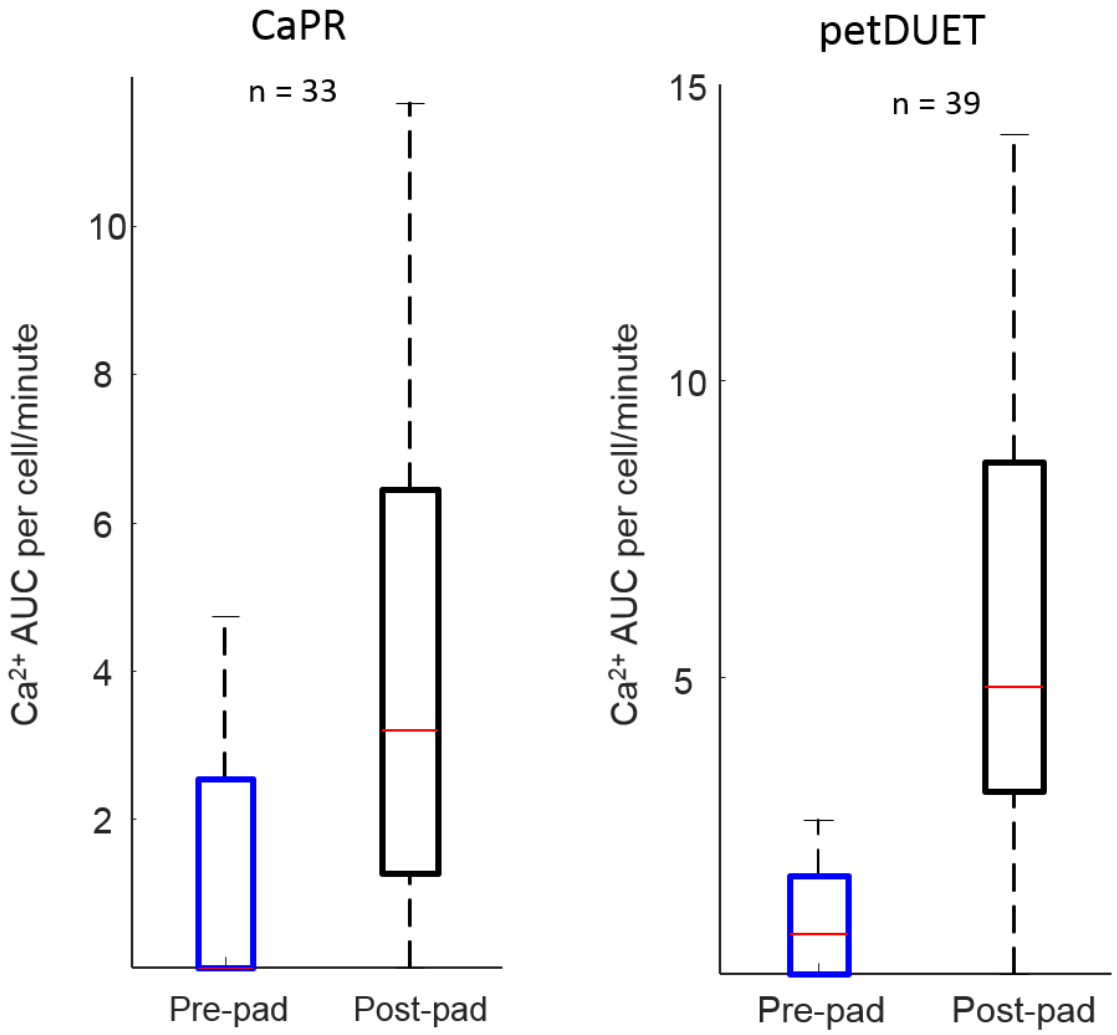

Supplementary Figure 13 – Mechanically induced calcium transients are detected in both the fused CaPR construct as well as the cytoplasmic GCaMP6f with transmembrane PROPS. Boxplots of calcium transients before and after mechanical stimulation in cells expressing CaPR (A), and petDUET GCaMP6f and PROPS (B) constructs. These are similar to experiments in Fig. 3A-D.

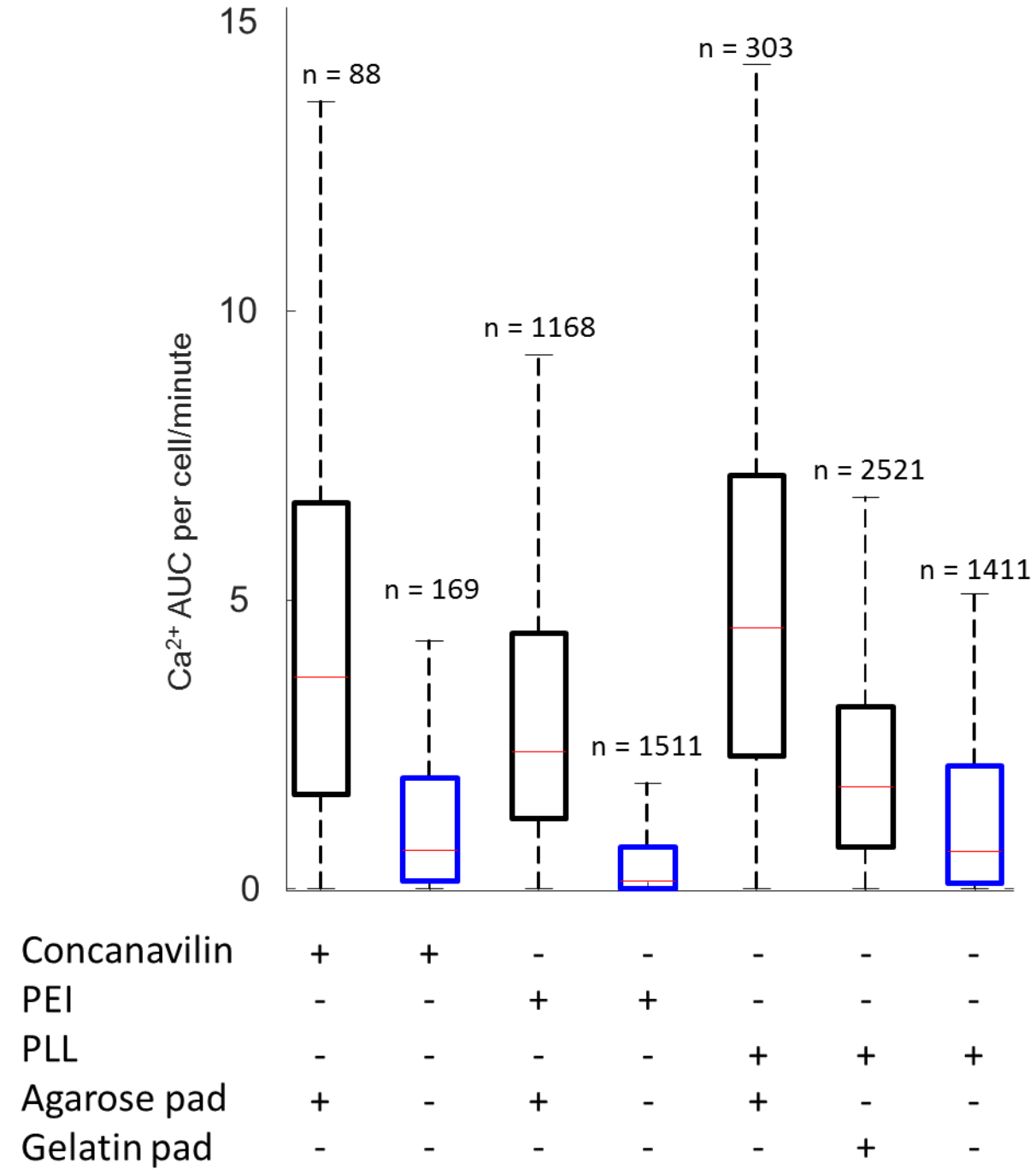

Supplementary Figure 14 – Mechanically induced calcium transients are substrate independent. Calcium AUC measurements under an agarose pad adhered by concanavilin or polyethylenimine (black box plots) also show increased calcium flux compared to liquid adhered cells (blue/black box plots). Gelatin also induces increased calcium flux. Red line indicates median, blue/black box indicates 75/25%, and black dashed lines indicate 90/10% of the maxima. Outliers were analyzed but not shown.

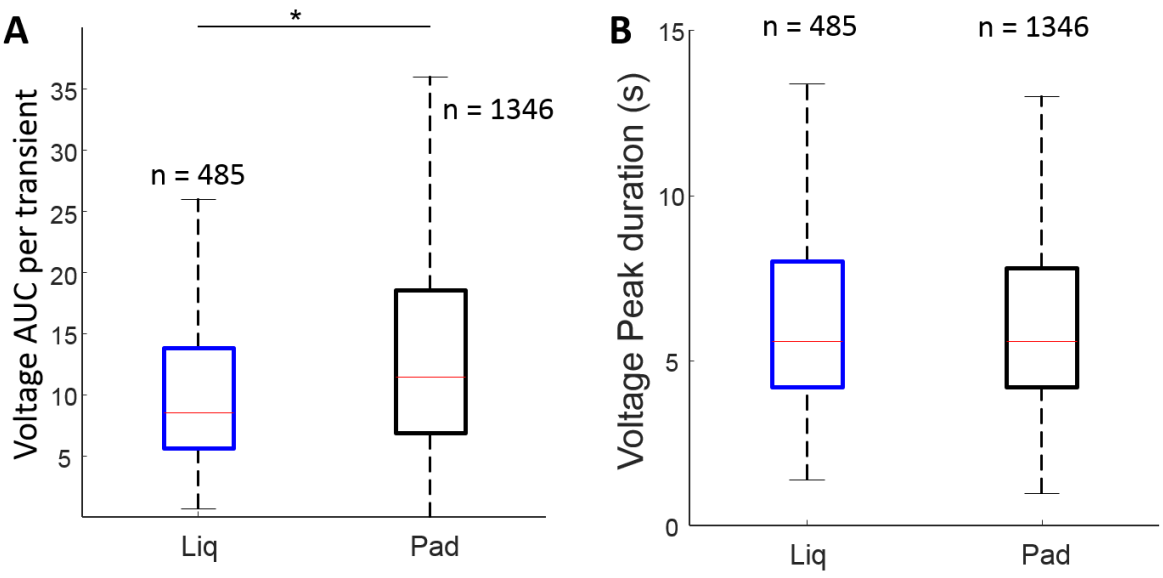

Supplementary Figure 15 – Voltage AUC and duration of voltage transients in the different mechanical environments. (A) Voltage AUC in the adhered pad condition increases as compared to the adhered liquid state by 38%. * represents $p < .001$ in an unpaired t-test with unequal variance. (B) The duration of individual voltage transients measured in the adhered pad condition show no difference compared to adhered liquid conditions. In each case, red line indicates median, blue/black box indicates 75/25%, and black dashed lines indicate 90/10% of the maxima. Outliers were analyzed but not shown.

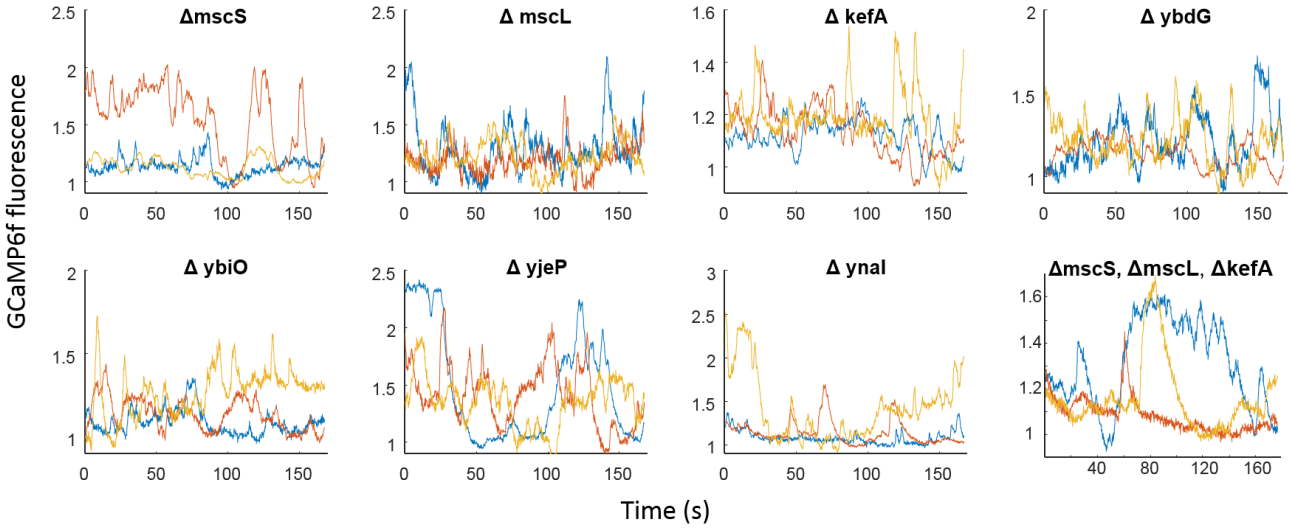

Supplementary Figure 16 - Calcium traces measured from individual knockouts of mechanosensitive channels. For each knockout, GCaMP expressing cells were measured from knockouts of the Keio collection under an agarose pad. The triple knockout has each of the three most highly expressed mechanosensitive channels knocked out. Each color represents a single cell. No single knockout eliminated calcium transients.

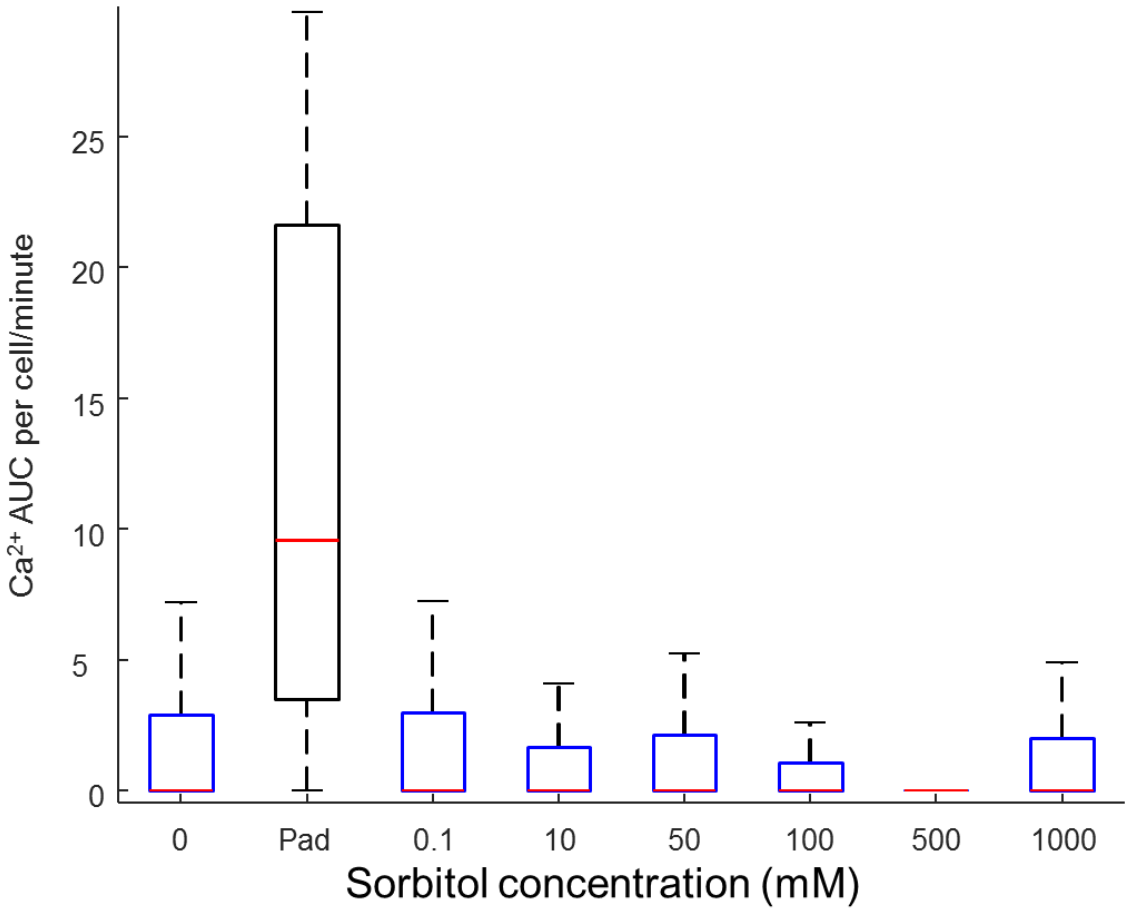

Supplementary Figure 17 – Osmotic pressure does not induce calcium transients. The calcium AUC was measured from CaPR expressing cells under an agarose pad and varying concentrations of sorbitol to alter osmotic pressure. Red line indicates median, blue/black box indicates 75/25%, and black dashed lines indicate 90/10% of the maxima. Outliers were analyzed but not shown.

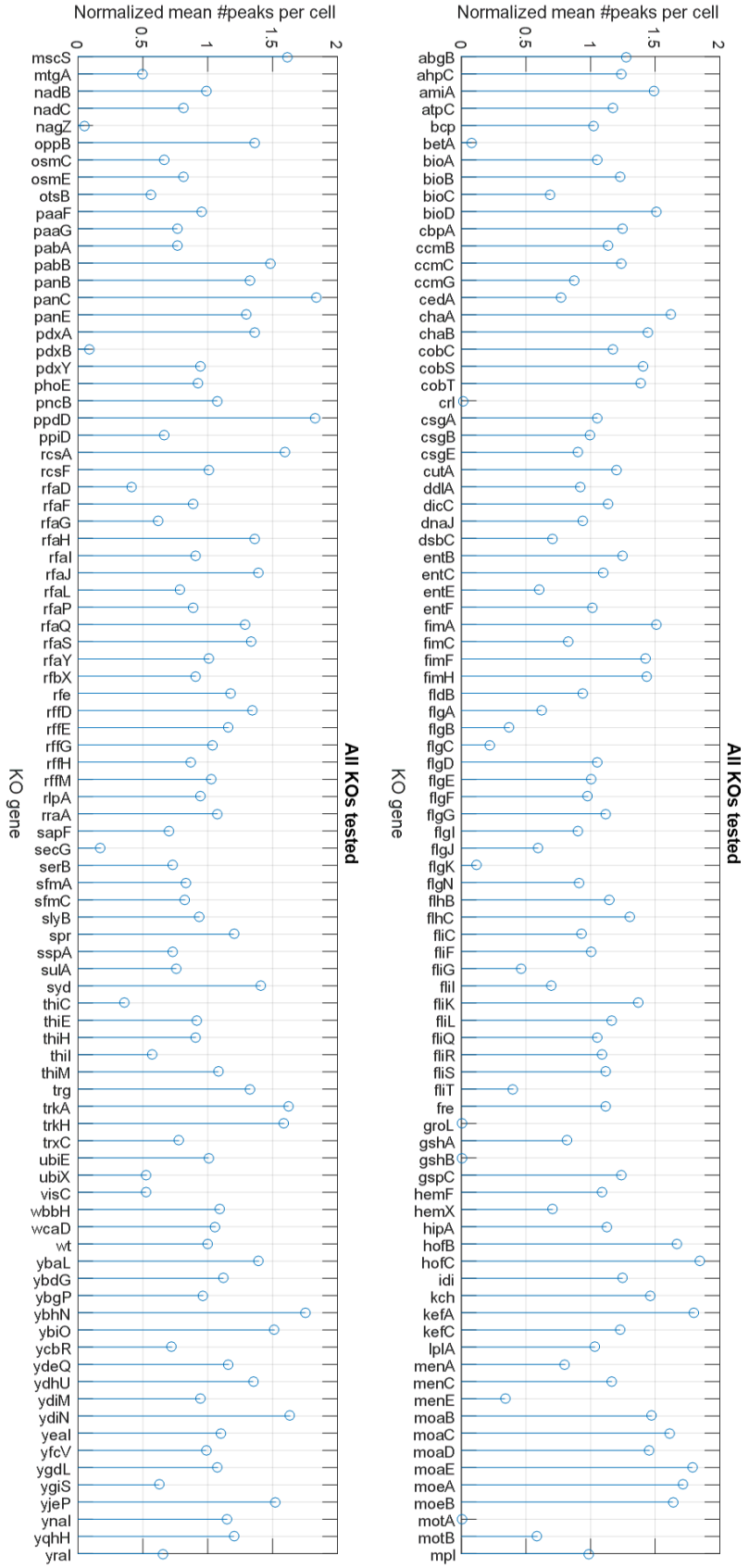

Supplementary Figure 18 - Calcium AUC measurements from 175 knockouts from the Keio collection. Each plot shows the mean calcium AUC for a population of cells from each knockout. The calcium AUC is normalized to the WT levels.

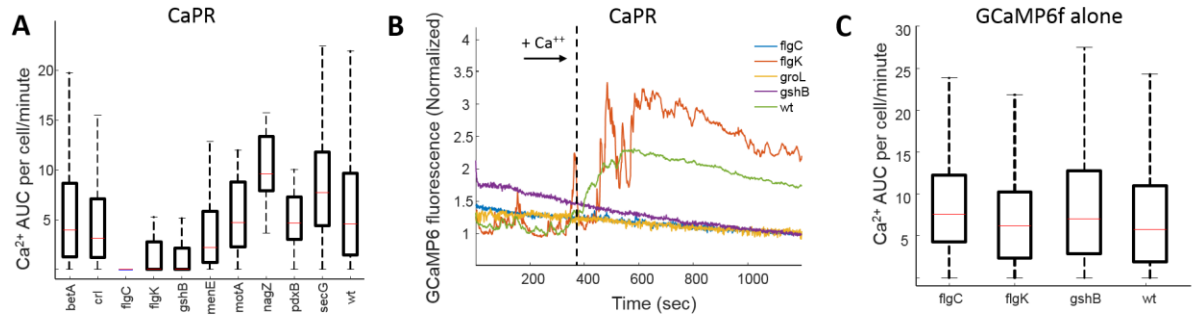

Supplementary Figure 19 – Verification of the initial hits from the knockout screen. (A) A retest of the 10 knockouts using the CaPR construct. Each box plot shows the calcium AUC per minute for the cells from that genotype. Red line indicates median, black box indicates 75/25%, and black dashed lines indicate 90/10% of the maxima. Outliers were analyzed but not shown. (B) GCaMP6 fluorescence (measured with the fused CaPR construct) for knockouts upon the addition of external calcium. Wildtype (green) and flgK knockout (red) cells all increase fluorescence upon addition of external calcium. The three knockouts (flgC, groL, gshB) did not respond indicating the sensor is not active. (C) The same 3 knockouts with Ca AUC measured using a cytoplasmic GCaMP6 sensor. Each of the knockouts was capable of generating calcium transients under an agarose pad. Red line indicates median, black box indicates 75/25%, and black dashed lines indicate 90/10% of the maxima. Outliers were analyzed but not shown.

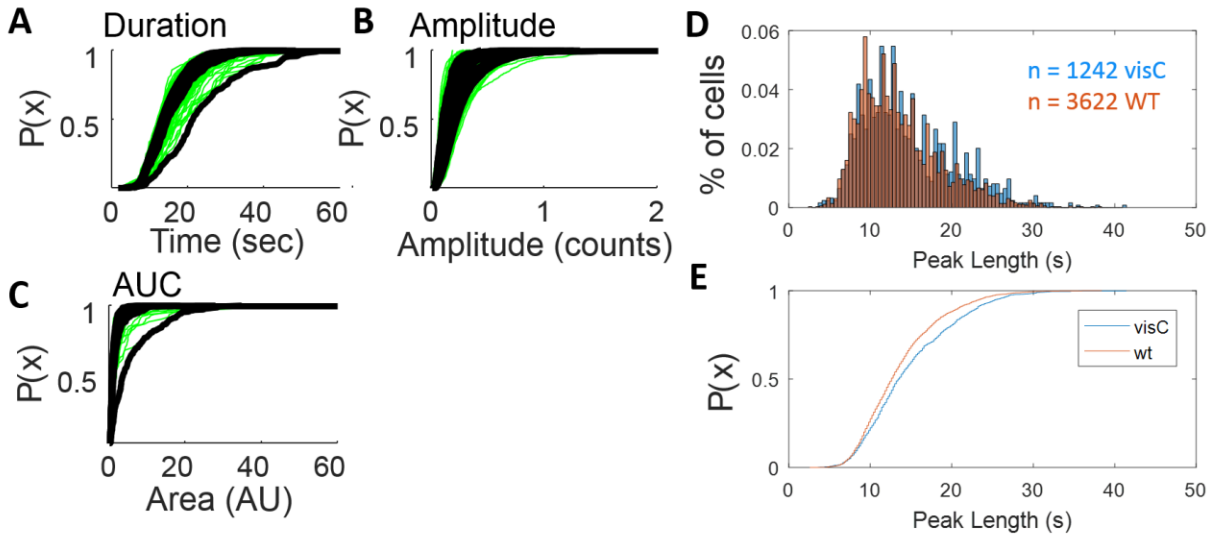

Supplementary Figure 20 – Empirical cumulative distribution function (CDF) analysis of 175 knockouts (green) and wildtype (black) calcium transients. In each knockout, every transient was measured for the (A) duration, (B) amplitude, and (C) area under the curve. To calculate deviants the standard deviation at each point on the x-axis was calculated for the WT, and then any curve that had a point outside 3x the WT standard deviation was considered. For clarity, we removed knockouts that had fewer than 15 cumulative transients, and any movies that were contaminated by drift. After replication, visC remained outside our selection criteria. (D) Histogram of peak lengths for WT (orange, 3622 transients) and VisC knockout (blue, 1242 transients). The visC knockout increased the mean peak length duration from 12.6 to 14.8 seconds. (E) Replication of the empirical cumulative distribution function for WT and visC showing visC has longer peaks than WT.

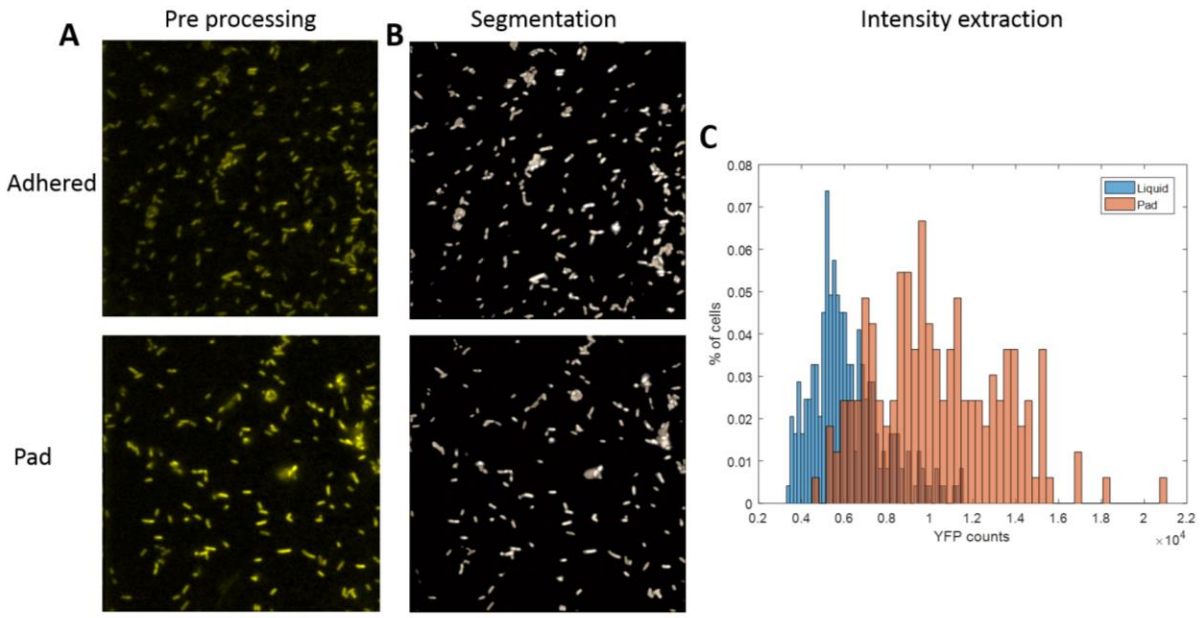

Supplementary Figure 21 – Analysis flow of YFP expression data. The same strain of cells was imaged in an adhered state, and either submerged in liquid or with an agarose pad. Preprocessing consisted of illumination correction and background subtraction. Individual cells were then segmented using a modified marker controlled watershed. From the segmented images, cell intensities were calculated using the mean of all pixels from each cell, and plotted in a histogram.

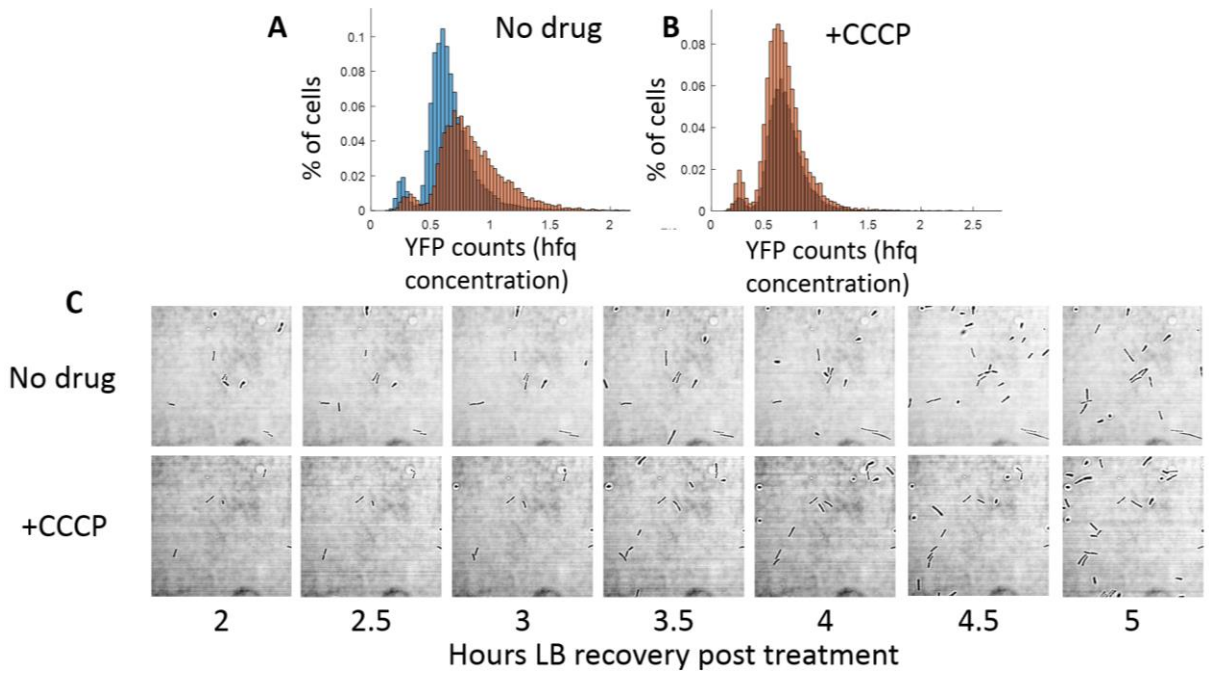

Supplementary Figure 22 – CCCP treatment blocks mechanosensitive hfq protein concentration differences, but does not kill the cells. (A) Distributions in the absence of CCCP show mechanically induced increases in hfq concentration. (B) Distributions show no difference between adhered liquid and adhered pad conditions in the presence of 10 μM CCCP. (C) Adhered bacteria can continue to grow and divide after no treatment (top) and CCCP (bottom) treatment when grown in LB.

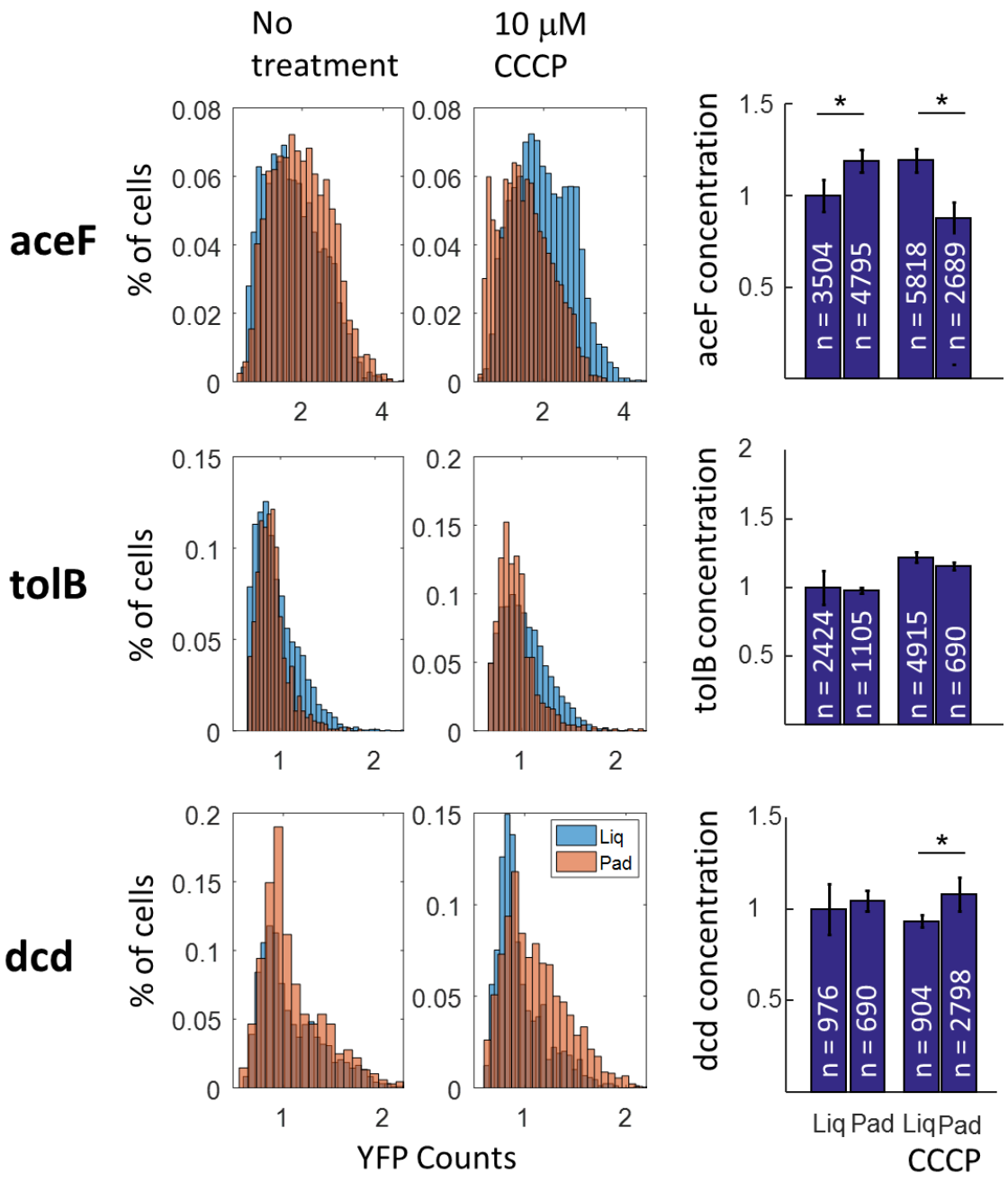

Supplementary Figure 23 – Additional protein concentration differences in the presence of CCCP. For each gene, we tested the pad vs glass adhered conditions which replicated previous measurements, as well as pad vs glass adhered in the presence of CCCP. The raw histograms show glass adhered (blue) or under an agarose pad (red). Bar graphs show the mean value for a normal distribution fit to the data. The error bars represent the 99.9% confidence interval for the mean fit. The number of cells used for each measurement is displayed in the bar. *represents a p value < .001.

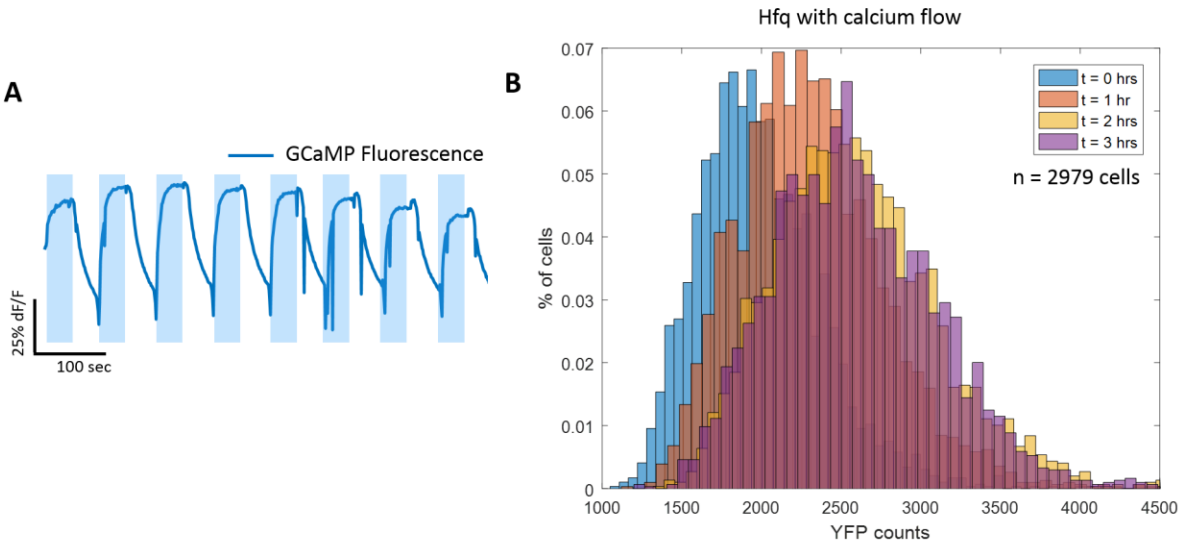

Supplementary Figure 24 – External calcium increases the intracellular calcium levels in *E. coli*, which are capable of driving hfq concentration increases. (A) Mean GCaMP fluorescence levels upon flow of 5 mM external calcium concentration for 30 seconds (blue shading), followed by 0 mM calcium for 30 seconds. Cytoplasmic levels oscillated in phase with external calcium levels. (B) Raw data shown for figure 4F. Expression of hfq before flow (blue) and after 1 hour (red), 2 hours (yellow), or 3 hours (purple) hours of oscillating external calcium flow.

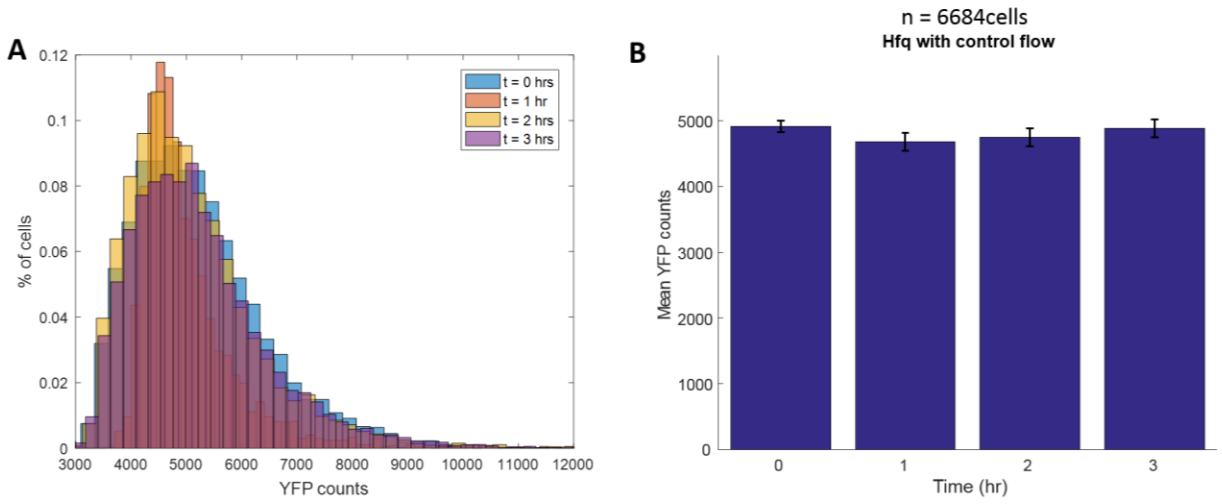

Supplementary Figure 25 – Flow in the absence of calcium does not alter hfq expression. (A) Cells immobilized on glass with PLL were exposed to alternating flow every 30 seconds, but without a difference in external calcium concentration. Venus fluorescence was measured across a population of cells (n = 6684 cells). (B) Mean values for a normal fit to the distributions. The error bars represent the 99.9% confidence interval for a Gaussian fit.

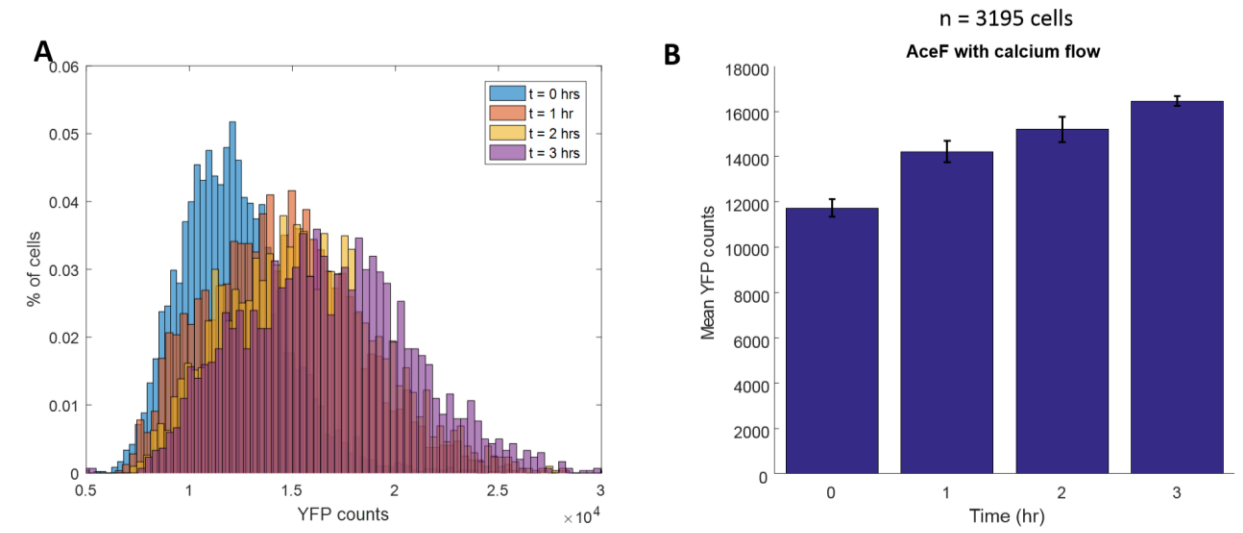

Supplementary Figure 26 – AceF increases in the presence of alternating calcium flow. (A) Cells immobilized on glass with PLL were exposed to alternating flow with 0 mM or 5 mM external calcium every 30 seconds. Venus fluorescence was measured across a population of cells (n = 3195 cells). (B) Mean values for a normal fit to the distributions. The error bars represent the 99.9% confidence interval for a Gaussian fit.

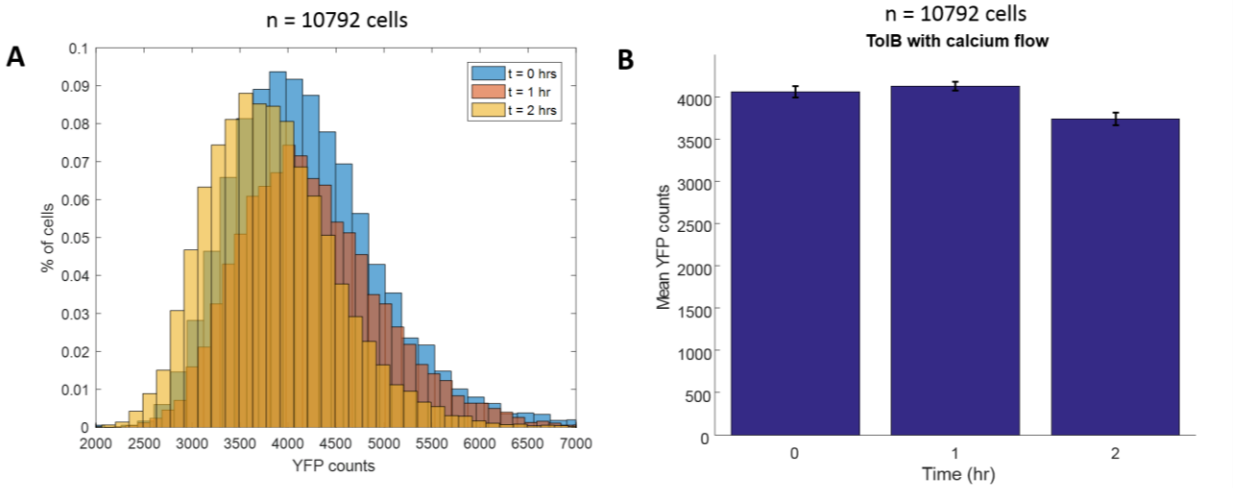

Supplementary Figure 27 – TolB decreases in the presence of alternating calcium flow. (A) Cells immobilized on glass with PLL were exposed to alternating flow with 0 mM or 5 mM external calcium every 30 seconds. Venus fluorescence was measured across a population of cells (n = 10,792 cells). (B) Mean values for a normal fit to the distributions. The error bars represent the 99.9% confidence interval for a Gaussian fit.

Supplementary Tables:

Sensor	Signal	Emission wavelnegth	Result in *E. coli*
RCaMP1h	Calcium	580 nm	No fluorescent expression
jRCaMP1	Calcium	580 nm	No fluorescent expression
jRCaMP2	Calcium	580 nm	No fluorescent expression
jRGECO	Calcium	580 nm	No fluorescent expression
pHuji	pH	580 nm	Blue light induced transients
pHRed	pH	580 nm	No fluorescent expression

Table S1 – Non-functional red sensors in *E. coli*.

ORF	Alternative Names	Product
'abgB'	'b1337,ECK1333,f481,JW1331,ydaI'	'p-aminobenzoyl-glutamate hydrolase, B subunit'
'ahpC'	'b0605,ECK0599,JW0598,tpx'	'alkyl hydroperoxide reductase, C22 subunit'
'amiA'	'b2435,ECK2430,JW2428,yfeE'	'N-acetylmuramoyl-l-alanine amidase I'
'atpC'	'b3731,ECK3724,JW3709,papG,uncC'	'F1 sector of membrane-bound ATP synthase, epsilon subunit'
'bcp'	'b2480,ECK2476,JW2465'	'peroxiredoxin; thiol peroxidase, thioredoxin-dependent'
'betA'	'b0311,ECK0309,JW0303'	'choline dehydrogenase, a flavoprotein'
'bioA'	'b0774,ECK0763,JW0757'	'7,8-diaminopelargonic acid synthase, PLP-dependent'
'bioB'	'b0775,ECK0764,JW0758'	'biotin synthase'
'bioC'	'b0777,ECK0766,JW0760'	'malonyl-CoA methyltransferase, SAM-dependent'
'bioD'	'b0778,ECK0767,JW0761'	'dethiobiotin synthetase'
'cbpA'	'b1000,ECK0991,f306,JW0985'	'curved DNA-binding protein, DnaJ homologue that functions as a co-chaperone of DnaK'
'ccmB'	'b2200,ECK2192,JW2188,yejV'	'heme exporter subunit'
'ccmC'	'b2199,ECK2191,JW2187,yejT,yejU'	'heme exporter subunit'
'dsbE'	'b2195,ccmG,dsbE,ECK2187,JW2183,yejQ'	'periplasmic thioredoxin of cytochrome c-type biogenesis'
'cedA'	'b1731,ECK1729,f87,JW1720,ydjP'	'cell division modulator'
'chaA'	'b1216,ECK1210,JW1207'	'calcium/sodium:proton antiporter'
'chaB'	'b1217,ECK1211,JW1208'	'cation transport regulator'
'cobC'	'b0638,ECK0631,JW0633,phpB'	'putative alpha-ribazole-5''-P phosphatase'
'cobS'	'b1992,ECK1987,JW1970'	'cobalamin synthase'
'cobT'	'b1991,ECK1986,JW1969'	'nicotinate-nucleotide--dimethylbenzimidazole phosphoribosyltransferase'
'crl'	'b0240,ECK0241,JW0230'	'sigma factor-binding protein, stimulates RNA polymerase holoenzyme formation'

'csgA'	'agfA,b1042,ECK1028,JW1025'	'curlin subunit, amyloid curli fibers, cryptic'
'csgB'	'agfB,b1041,ECK1027,JW1024'	'curlin nucleator protein, minor subunit in curli complex'
'csgE'	'agfE,b1039,ECK1025,JW1022'	'curlin secretion specificity factor'
'cutA'	'b4137,cutA1,cycY,ECK4131,f112,JW4097'	'divalent-cation tolerance protein, copper sensitivity'
'ddlA'	'b0381,ECK0376,JW0372'	'D-alanine-D-alanine ligase A'
'dicC'	'b1569,ECK1563,ftsT,JW1561'	'Qin prophage; DNA-binding transcriptional regulator for DicB'
'dnaJ'	'b0015,ECK0015,faa,groA,groB,groC,groP,grpC,JW0014'	'chaperone Hsp40, co-chaperone with DnaK'
'dsbC'	'b2893,ECK2888,JW2861,xprA'	'protein disulfide isomerase II'
'entB'	'b0595,ECK0588,entG,JW0587'	'isochorismatase'
'entC'	'b0593,ECK0586,fepF,JW0585'	'isochorismate synthase 1'
'entE'	'b0594,ECK0587,JW0586'	'2,3-dihydroxybenzoate-AMP ligase component of enterobactin synthase multienzyme complex'
'entF'	'b0586,ECK0579,JW0578'	'enterobactin synthase multienzyme complex component, ATP-dependent'
'fimA'	'b4314,ECK4305,fimD,JW4277,pilA'	'major type 1 subunit fimbrin (pilin)'
'fimC'	'b4316,ECK4307,JW4279,pil,pilB'	'periplasmic chaperone'
'fimF'	'b4318,ECK4309,JW4281,pilD'	'minor component of type 1 fimbriae'
'fimH'	'b4320,ECK4311,JW4283,pilE'	'minor component of type 1 fimbriae'
'fldB'	'b2895,ECK2890,JW2863'	'flavodoxin 2'
'flgA'	'b1072,ECK1057,flaU,JW1059'	'assembly protein for flagellar basal-body periplasmic P ring'
'flgB'	'b1073,ECK1058,flbA,JW1060'	'flagellar component of cell-proximal portion of basal-body rod'
'flgC'	'b1074,ECK1059,flaW,JW1061'	'flagellar component of cell-proximal portion of basal-body rod'
'flgD'	'b1075,ECK1060,flaV,JW1062,o231'	'flagellar hook assembly protein'

'flgE'	'b1076,ECK1061,flaK,JW1063'	'flagellar hook protein'
'flgF'	'b1077,ECK1062,flaX,JW1064'	'flagellar component of cell-proximal portion of basal-body rod'
'flgG'	'b1078,ECK1063,flaL,JW1065'	'flagellar component of cell-distal portion of basal-body rod'
'flgI'	'b1080,ECK1065,flaM,JW1067'	'putative flagellar basal body protein'
'flgJ'	'b1081,ECK1066,flaZ,JW1068,o313'	'muramidase'
'flgK'	'b1082,ECK1067,flaS,JW1069'	'flagellar hook-filament junction protein 1'
'flgN'	'b1070,ECK1055,JW1057'	'export chaperone for FlgK and FlgL'
'flhB'	'b1880,ECK1881,f382b,flaG,JW1869,yecQ'	'flagellin export apparatus, substrate specificity protein'
'flhC'	'b1891,ECK1892,flaI,JW1880'	'DNA-binding transcriptional dual regulator with FlhD'
'fliC'	'b1923,ECK1922,flaF,H,hag,JW1908'	'flagellar filament structural protein (flagellin)'
'fliF'	'b1938,ECK1936,flaAII.1,flaBI,JW1922,o552'	'flagellar basal-body MS-ring and collar protein'
'fliG'	'b1939,ECK1937,flaAII.2,flaBII,JW1923'	'flagellar motor switching and energizing component'
'fliI'	'b1941,ECK1939,flaC,JW1925'	'flagellum-specific ATP synthase'
'fliK'	'b1943,ECK1941,flaE,JW1927'	'flagellar hook-length control protein'
'fliL'	'b1944,cheC1,ECK1942,flaAI,flaQI,JW1928'	'flagellar biosynthesis protein'
'fliQ'	'b1949,ECK1947,flaQ,JW1933'	'flagellar biosynthesis protein'
'fliR'	'b1950,ECK1948,flaP,JW1934'	'flagellar export pore protein'
'fliS'	'b1925,ECK1924,JW1910'	'flagellar protein potentiates polymerization'
'fliT'	'b1926,ECK1925,JW1911'	'putative chaperone'
'fre'	'b3844,ECK3836,fadI,flrD,frlD,fsrC,hsm-6,JW3820,o233,ubiB'	'NAD(P)H-flavin reductase'
'groL'	'b4143,ECK4137,groEL,JW4103,mopA,o548'	'Cpn60 chaperonin GroEL, large subunit of GroESL'
'gshA'	'b2688,ECK2683,gshI,JW2663'	'glutamate-cysteine ligase'

'gshB'	'b2947,ECK2942,gsh-II,JW2914'	'glutathione synthetase'
'gspC'	'b3324,ECK3311,JW3286,o271,yheE'	'general secretory pathway component, cryptic'
'hemF'	'b2436,ECK2431,JW2429,popB,sec'	'coproporphyrinogen III oxidase'
'hemX'	'b3803,ECK3797,JW3775'	'putative uroporphyrinogen III methyltransferase'
'hipA'	'b1507,ECK1500,JW1500'	'EF-Tu kinase; serine protein kinase required for persister formation; toxin of HipAB TA pair'
'hofB'	'b0107,ECK0106,hopB,JW0103'	'conserved protein with nucleoside triphosphate hydrolase domain'
'hofC'	'b0106,ECK0105,f400,hopC,JW0102,yacD'	'assembly protein in type IV pilin biogenesis, transmembrane protein'
'idi'	'b2889,ECK2884,JW2857,o182,o182a,ygfV'	'isopentenyl diphosphate isomerase'
'kch'	'b1250,ECK1244,JW1242'	'voltage-gated potassium channel'
'mscK'	'aefA,b0465,ECK0459,JW0454,kefA,mscK,o1120,o1120a,pnuH'	'mechanosensitive channel protein, intermediate conductance, K+ regulated'
'kefC'	'b0047,ECK0048,JW0046,trkC'	'potassium:proton antiporter'
'lplA'	'b4386,ECK4378,f338,JW4349,slr,yjjF'	'lipoate-protein ligase A'
'menA'	'b3930,ECK3922,f308,JW3901,yiiW'	'1,4-dihydroxy-2-naphthoate octaprenyltransferase'
'menC'	'b2261,ECK2255,f320,JW2256'	'O-succinylbenzoyl-CoA synthase'
'menE'	'b2260,ECK2254,JW2255'	'O-succinylbenzoate-CoA ligase'
'moaB'	'b0782,ECK0771,JW0765'	'molybdopterin biosynthesis protein B'
'moaC'	'b0783,ECK0772,JW0766,o161'	'molybdopterin biosynthesis, protein C'
'moaD'	'b0784,chlM,ECK0773,JW0767'	'molybdopterin synthase, small subunit'
'moaE'	'b0785,ECK0774,JW0768'	'molybdopterin synthase, large subunit'
'moeA'	'b0827,bisB,chlE,ECK0817,JW0811,narE'	'molybdopterin molybdenumtransferase; molybdopterin biosynthesis protein'
'moeB'	'b0826,chlN,ECK0816,JW0810'	'molybdopterin synthase sulfurylase'
'motA'	'b1890,ECK1891,flaJ,JW1879'	'proton conductor component of flagella

		motor'
'motB'	'b1889,ECK1890,flaJ,JW1878'	'protein that enables flagellar motor rotation'
'mpl'	'b4233,ECK4228,JW4192,o457,tpl,yjfG'	'UDP-N-acetylmuramate:L-alanyl-gamma-D-glutamyl- meso-diaminopimelate ligase'
'mscS'	'b2924,ECK2920,JW2891,yggB'	'mechanosensitive channel protein, small conductance'
'mtgA'	'b3208,ECK3197,f242,JW3175,mgt,yrbM'	'biosynthetic peptidoglycan transglycosylase'
'nadB'	'b2574,ECK2572,JW2558,nic,nicB'	'quinolinate synthase, L-aspartate oxidase (B protein) subunit'
'nadC'	'b0109,ECK0108,JW0105'	'quinolinate phosphoribosyltransferase'
'nagZ'	'b1107,ECK1093,JW1093,o341,ycfO'	'beta N-acetyl-glucosaminidase'
'oppB'	'b1244,ECK1238,JW1236,stkB'	'oligopeptide transporter subunit'
'osmC'	'b1482,ECK1476,JW1477'	'lipoyl-dependent Cys-based peroxidase, hydroperoxide resistance; salt-shock inducible membrane protein; peroxiredoxin'
'osmE'	'anr,b1739,ECK1737,JW1728'	'DNA-binding transcriptional activator'
'otsB'	'b1897,ECK1896,JW1886,otsP'	'trehalose-6-phosphate phosphatase, biosynthetic'
'paaF'	'b1393,ECK1390,JW1388,o255,ydbR,ydbS'	'2,3-dehydroadipyl-CoA hydratase'
'paaG'	'b1394,ECK1391,JW1389,o262,o262b,ydbT'	'1,2-epoxyphenylacetyl-CoA isomerase, oxepin-CoA-forming'
'pabA'	'b3360,ECK3348,f187,JW3323'	'aminodeoxychorismate synthase, subunit II'
'pabB'	'b1812,ECK1810,JW1801'	'aminodeoxychorismate synthase, subunit I'
'panB'	'b0134,ECK0133,JW0130,panA'	'3-methyl-2-oxobutanoate hydroxymethyltransferase'
'panC'	'b0133,ECK0132,JW0129'	'pantothenate synthetase'
'panE'	'apbA,b0425,ECK0419,f303,JW0415'	'2-dehydropantoate reductase, NADPH-specific'
'pdxA'	'b0052,ECK0053,JW0051'	'4-hydroxy-L-threonine phosphate dehydrogenase, NAD-dependent'

'pdxB'	'b2320,ECK2314,JW2317'	'erythronate-4-phosphate dehydrogenase'
'pdxY'	'b1636,ECK1632,f287,f287b,JW1628,ydgS'	'pyridoxamine kinase'
'phoE'	'b0241,ECK0242,JW0231,ompE'	'outer membrane phosphoporin protein E'
'pncB'	'b0931,ECK0922,JW0914'	'nicotinate phosphoribosyltransferase'
'ppdD'	'b0108,ECK0107,JW0104'	'putative major pilin subunit'
'ppiD'	'b0441,ECK0435,JW0431,o623,ybaU'	'periplasmic folding chaperone, has an inactive PPIase domain'
'rcsA'	'b1951,cpsR,ECK1949,JW1935'	'DNA-binding transcriptional activator, co-regulator with RcsB'
'rcsF'	'b0196,ECK0196,JW0192'	'putative outer membrane protein, signal'
'hldD'	'b3619,ECK3609,gmhD,hldD,htrM,JW3594,nbsB,rfaD,waaD'	'ADP-L-glycero-D-mannoheptose-6-epimerase, NAD(P)-binding'
'waaF'	'b3620,ECK3610,JW3595,o348,rfaF,waaF'	'ADP-heptose:LPS heptosyltransferase II'
'waaG'	'b3631,ECK3621,JW3606,rfaG,waaG'	'glucosyltransferase I'
'rfaH'	'b3842,ECK3834,hlyT,JW3818,sfrB'	'DNA-binding transcriptional antiterminator'
'waaR'	'b3627,ECK3617,JW3602,rfaI,waaI,waaJ'	'UDP-D-galactose:(glucosyl)lipopolysaccharide-alpha-1,3-D-galactosyltransferase'
'waaJ'	'b3626,ECK3616,JW3601,rfaJ,waaJ,waaR'	'UDP-D-glucose:(galactosyl)lipopolysaccharide glucosyltransferase'
'waaL'	'b3622,ECK3612,JW3597,o419,rfaL,waaL'	'O-antigen ligase'
'waaP'	'b3630,ECK3620,JW3605,rfaP,waaP'	'kinase that phosphorylates core heptose of lipopolysaccharide'
'waaQ'	'b3632,ECK3622,f344,JW3607,rfaQ,waaQ'	'lipopolysaccharide core biosynthesis protein'
'waaS'	'b3629,ECK3619,f311,JW3604,rfaS,waaS'	'lipopolysaccharide core biosynthesis protein'
'waaY'	'b3625,ECK3615,f232,JW3600,rfaY,waaY'	'lipopolysaccharide core biosynthesis protein'
'wzxB'	'b2037,ECK2031,JW2022,rfbX,wzx,wzx	'putative polisoprenol-linked O-antigen

	B'	transporter'
'wecA'	'b3784,ECK3776,JW3758,o367,rfe,wecA'	'UDP-GlcNAc:undecaprenylphosphate GlcNAc-1-phosphate transferase'
'wecC'	'b3787,ECK3779,JW5599,o420,rff,rffD,wecC'	'UDP-N-acetyl-D-mannosaminuronic acid dehydrogenase'
2x1 cell	2x1 cell	2x1 cell
'rffG'	'b3788,ECK3780,JW5598,rff,rffE'	'dTDP-glucose 4,6-dehydratase'
'rffH'	'b3789,ECK3781,JW3763,o293,yifG'	'glucose-1-phosphate thymidylyltransferase'
'wecG'	'b3794,ECK3787,JW3770,o246,rff,rffM,wecG'	'UDP-N-acetyl-D-mannosaminuronic acid transferase'
'rlpA'	'b0633,ECK0626,JW0628'	'septal ring protein, suppressor of prc, minor lipoprotein'
'rraA'	'b3929,ECK3921,f161,JW3900,menG,yiiV'	'ribonuclease E (RNase E) inhibitor protein'
'sapF'	'b1290,ECK1285,JW1283'	'antimicrobial peptide transport ABC system ATP-binding protein'
'secG'	'b3175,ECK3164,JW3142,prlH'	'preprotein translocase membrane subunit'
'serB'	'b4388,ECK4380,JW4351'	'3-phosphoserine phosphatase'
'sfmA'	'b0530,ECK0523,fimA,JW0519,o191,o191a'	'putative fimbrial-like adhesin protein'
'sfmC'	'b0531,ECK0524,fimC,JW0520,o230,o230a'	'pilin chaperone, periplasmic'
'slyB'	'b1641,ECK1637,JW1633,o155,o155a'	'outer membrane lipoprotein'
'spr'	'b2175,ECK2169,JW2163,o188,yeiV'	'mutational suppressor of prc thermosensitivity, outer membrane lipoprotein'
'sspA'	'b3229,ECK3218,f212,JW3198,pog,ssp'	'stringent starvation protein A'
'sulA'	'b0958,ECK0949,JW0941,sfiA'	'SOS cell division inhibitor'
'syd'	'b2793,ECK2788,JW2764,ydr'	'secY-interacting protein'
'thiC'	'b3994,ECK3986,JW3958'	'thiamin (pyrimidine moiety) biosynthesis protein'

'thiE'	'b3993,ECK3985,f211,JW3957,thiA'	'thiamin phosphate synthase (thiamin phosphate pyrophosphorylase)'
'thiH'	'b3990,ECK3981,f377,JW3953,thiB'	'tyrosine lyase, involved in thiamin-thiazole moiety synthesis'
'thiI'	'b0423,ECK0417,JW0413,nuvA,o482,yajJ,yajK'	'tRNA s(4)U8 sulfurtransferase'
'thiM'	'b2104,ECK2097,f262,f262c,JW2091'	'hydoxyethylthiazole kinase'
'trg'	'b1421,ECK1415,JW1417,o546'	'methyl-accepting chemotaxis protein III, ribose and galactose sensor receptor'
'trkA'	'b3290,ECK3276,JW3251,o458,sapG'	'NAD-binding component of TrK potassium transporter'
'trkH'	'b3849,ECK3841,JW5576,o432,sapJ'	'potassium transporter'
'trxC'	'b2582,ECK2580,JW2566,o139,yfiG'	'thioredoxin 2'
'ubiE'	'b3833,ECK3827,JW5581,menG,menH,yigO'	'bifunctional2-octaprenyl-6-methoxy-1,4-benzoquinone methylase/ S-adenosylmethionine:2-DMK methyltransferase'
'ubiX'	'b2311,dedF,ECK2305,JW2308'	'3-octaprenyl-4-hydroxybenzoate carboxy-lyase'
'visC'	'b2906,ECK2901,JW2874'	'putative oxidoreductase with FAD/NAD(P)-binding domain'
'wbbH'	'b2035,ECK2029,f388,JW2020,rfc,wbbH,yefF'	'O-antigen polymerase'
'wcaD'	'b2056,ECK2050,f405,JW2041'	'putative colanic acid polymerase'
'ybaL'	'b0478,ECK0472,JW0467,ylaA'	'putative transporter with NAD(P)-binding Rossmann-fold domain'
'ybdG'	'b0577,ECK0569,JW0566,mscM,ybdG'	'mechanosensitive channel protein, miniconductance'
'ybgP'	'b0717,ECK0706,f242,JW0707'	'putative periplasmic pilus chaperone'
'ybhN'	'b0788,ECK0777,f318,f318c,JW0771'	'conserved inner membrane protein'
'ybiO'	'b0808,ECK0797,f786,JW5108'	'mechanosensitive channel protein, intermediate conductance'
'elfD'	'b0939,ECK0930,JW0922,o233,ycbR'	'putative periplasmic pilin chaperone'

'ydeQ'	'b1502,ECK1495,f304,f304a,fmlD,JW1496'	'putative fimbrial-like adhesin protein'
'ydhU'	'b1670,ECK1666,f261,f261a,JW1660'	'putative cytochrome'
'ydiM'	'b1690,ECK1688,JW1680,o404'	'inner membrane protein, predicted transporter'
'ydiN'	'b1691,ECK1689,JW5274,o423,o423b'	'inner membrane protein, predicted MFS superfamily transporter'
'yeaI'	'b1785,ECK1783,JW1774,o491'	'putative membrane-anchored diguanylate cyclase'
'yfcV'	'b2339,ECK2333,f187,f187b,JW2336'	'putative fimbrial-like adhesin protein'
'csdL'	'b2812,ECK2808,f268,f268b,JW2783,ygdL'	'sulfur acceptor for CsdA'
'ygiS'	'b3020,ECK3011,f535,JW2988'	'putative transporter subunit: periplasmic-binding component of ABC superfamily'
'mscM'	'b4159,ECK4155,JW4120,yjeP'	'mechanosensitive channel protein, miniconductance'
'ynaI'	'b1330,ECK1327,f343,JW1323'	'mechanosensitive channel protein, very small conductance'
'yqhH'	'b3014,ECK3006,JW2982,o85,o85a'	'outer membrane lipoprotein, Lpp paralog'
'yraI'	'b3143,ECK3131,JW3112,o231'	'putative periplasmic pilin chaperone'

Table S2 – Knockouts tested for calcium transients.

Actuator	**IC Signal**	**Outcome**
Channelrhodopsin 2	Cation channel	No membrane localization
CheRiff	Cation channel	No membrane localization
Np Halorhodopsin	Chloride pump	No light induced signal
Histamine gated chloride channel	Chloride channel	No chemical signal
Methylglyoxal	Calcium influx	No chemical signal

Table S3 – Failed optogenetic and chemogenetic actuators.

Supplementary Text:

Knockouts:

In lieu of the MSC family eliminating voltage gated calcium flux, we expanded our search for strains in the Keio library that eliminated calcium flux under an agarose pad. We chose knockouts of membrane components including genes associated with flagella, fimbriae, pili, and channels (SI Appendix, Table S2) because these knockouts seemed most likely to mediate a mechanical stimulus. A total of 175 knockout strains were measured expressing the constitutive CaPR plasmid (SI Appendix, Fig S18). For each knockout strain the mean AUC of calcium transients was calculated, and 10 knockouts were identified with < 30% of wildtype levels. Replicate testing showed 3 genes, groL, flgC, and gshB, continued to have low calcium transients. These knockout strains had very low GCaMP fluorescence and did not respond to external calcium addition, suggesting the knockout impaired sensor folding or stability (SI Appendix, Fig. S19). All three knockouts showed calcium transients when imaged with a cytoplasmic GCaMP6f construct and continued to grow under a pad when expressing CaPR, supporting this hypothesis. The 175 genes tested are unlikely to relay mechanosensation or the voltage gated calcium current.

Peak finding algorithm:

Finding peaks in the voltage data is accomplished through a sequence of classification and clustering steps. The algorithm is outlined as:

1. Normalize by dividing by standard deviation
2. Classify after Normalization using Poincare map
   a. Calculate Poincare map
   b. Find high and low threshold convex hulls
   c. Find centroids of convex hulls
   d. Find density near the centroid
   e. Calculate R-square of data inside convex hull
   f. Classify the time-series using a decision tree
3. Construct the peak region in the Poincare Map
4. Find the sequence of points above the Nth percentile of the points inside the high threshold convex hull, where this percentile defines the Peak Threshold.
5. If a sequence of points enters the peak region in the Poincare Map mark the entire sequence as a peak

The time series is classified into four categories by considering clusters of points in the Poincare plot (map) of the time series. For a time-series given by a sequence of values given by $y(t) = \{x(t_1), x(t_2), x(t_3), \ldots x(t_n)\}$ the Poincare map is formed by plotting ordered pairs of points $\left(x(t_{n-1}), x(t_n)\right)$. A 2-D histogram is calculated by binning the data $\left(x(t_{n-1}), x(t_n)\right)$ over a uniform 2-D grid. Approximate local densities are found by dividing the counts in the histogram by the total number of data points in the histogram. The density is re-scaled onto the interval [0, 1], to define the Poincare map, right column of the figure below. Finally, two density thresholds in the Poincare map (0 and 0.1 on the normalized density scale) form hierarchical clusters that are used to classify traces.

In the figure below, both the time series data and the corresponding Poincare map with hierarchical clusters are shown. Sample time series for each of the four classifications are shown in the left-hand column and the corresponding Poincare map in the right-hand column. The time series data has be rescaled by the standard deviation of the data. In order from top to bottom they are classified as a time series that is (i) quiet, (ii) a trend, (iii) peaks, or (iv) multiple modes. The black solid lines in the right-hand plots indicate the convex hull that defines clusters for two threshold values and the color of the scatter data indicates the relative density of the data, where a cool color corresponds to a low relative density and a warm color to a high relative density. Gray filled circular markers indicate the centroid of the high (0) and low (0.1) threshold clusters.

The time-series is classified into one of four categories, quiet, trend, peaks and multi-modal, by considering the convex hull of the density clusters. Specifically, if the centroid of the lowest threshold convex hull (largest cluster) is outside the convex hull of the higher threshold cluster (smaller cluster), indicates a time-series includes excursions from central mean value. The case where the centroid of the lowest threshold convex hull is inside the convex hull of the higher threshold cluster indicates the excursions from a mean value in the time-series is evenly distributed around a mean value throughout the domain of the time-series such as bi-modal data, i.e. where the data shifts from variations around a mean value to variations around a different mean value. In the case of the trend classification variations are superimposed on a slowly varying trend and in the quiet case variations are distributed evenly around a single mean value throughout the domain of the time-series. Finally, all the cases can be resolved by considering the R-square of the data inside the convex hull and the density of the data near the centroid. The following table summarizes the classification of the time series given the location of the centroids, the R-squared value of the data inside the centroids, and the density of the data near the centroid.

classification	Centroid low threshold cluster is inside high threshold cluster	R-squared	Density of data near centroid
Quiet	Yes	Low	Moderate to high
Trend	Yes	Moderate to high	Moderate to high
Peaks	No	Moderate to high	Moderate to high
Multi-modal	Yes	Moderate to high	Low

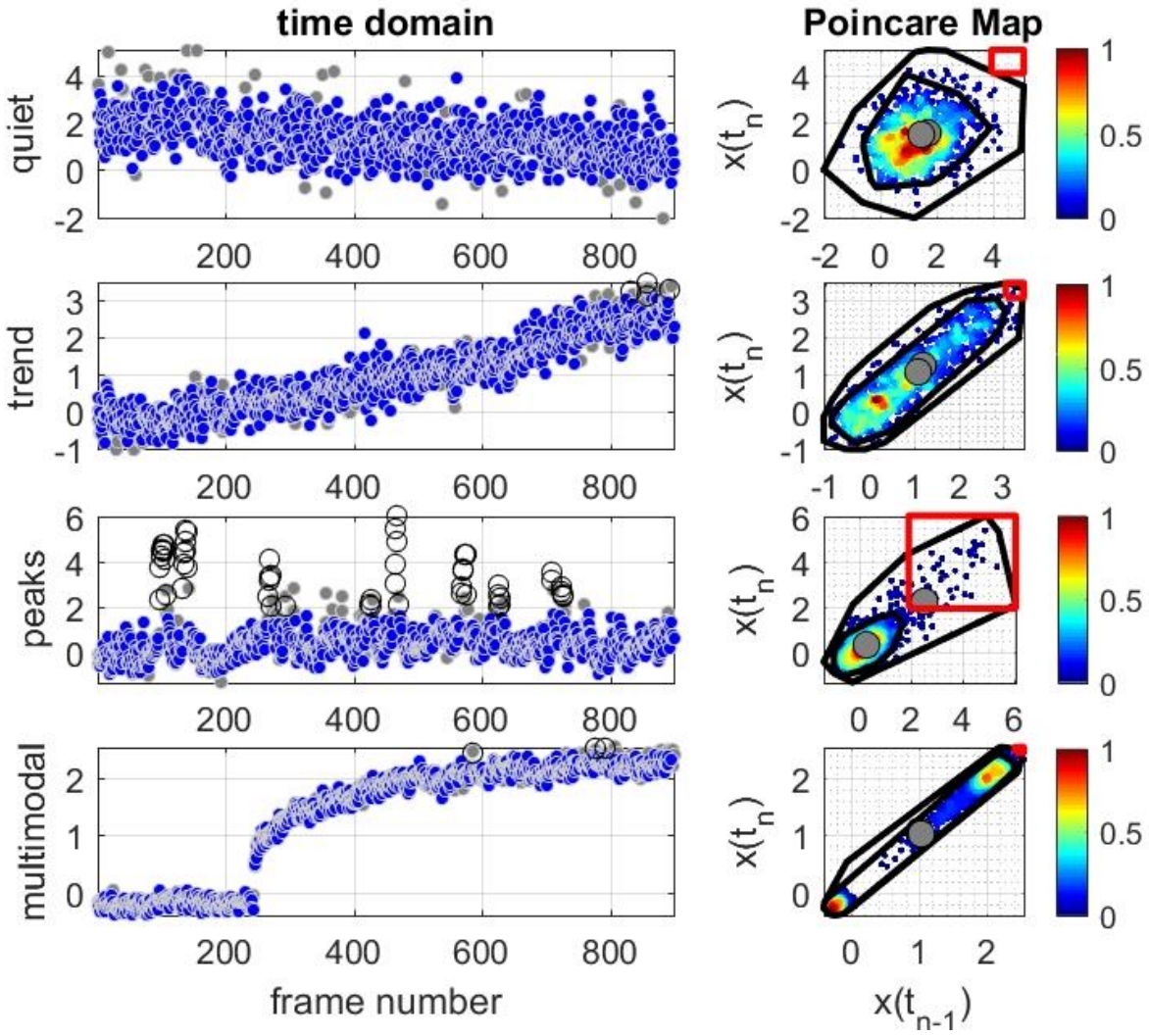

The red rectangle in the Poincare plot is used to find peaks in the time series. The time series data, in the figure above, is colored according to cluster membership in delay space. The blue points fall in the cluster defined by the innermost black contour (high threshold) in the Poincare plot. Black open circles fall inside the red box in the Poincare plot and are classified as potential peaks (see below), and gray data points are unassigned.

To find peaks, a polygonal region in the Poincare map is created outside the high threshold convex hull. Specifically, it is the rectangular region from the maximum x and y values of the Poincare plot to a point 95% the distance from the maximum x and y values in the Poincare map to the highest threshold cluster in the Poincare plot and is illustrated in the figure above as a red polygon. Data points inside the high threshold cluster in the Poincare map can be labeled in the time series. Visually, such points form a "band" in the time series, with unlabeled data above and below the band of data. A threshold value can be calculated by taking the Nth percentile of the data inside the high threshold cluster in the Poincare map. Sequences of points above the threshold value are found and are candidate peaks. Varying the threshold

value (see below) and comparing algorithm performance to a human trothed data set yielded an optimal value of 55%. A candidate sequence of data above the threshold is labeled a peak if any pair of points $\left(x(t_{n\text{-}1}),x(t_n)\right)$ in the sequence fall inside the peak region (red polygon) in the Poincare map.

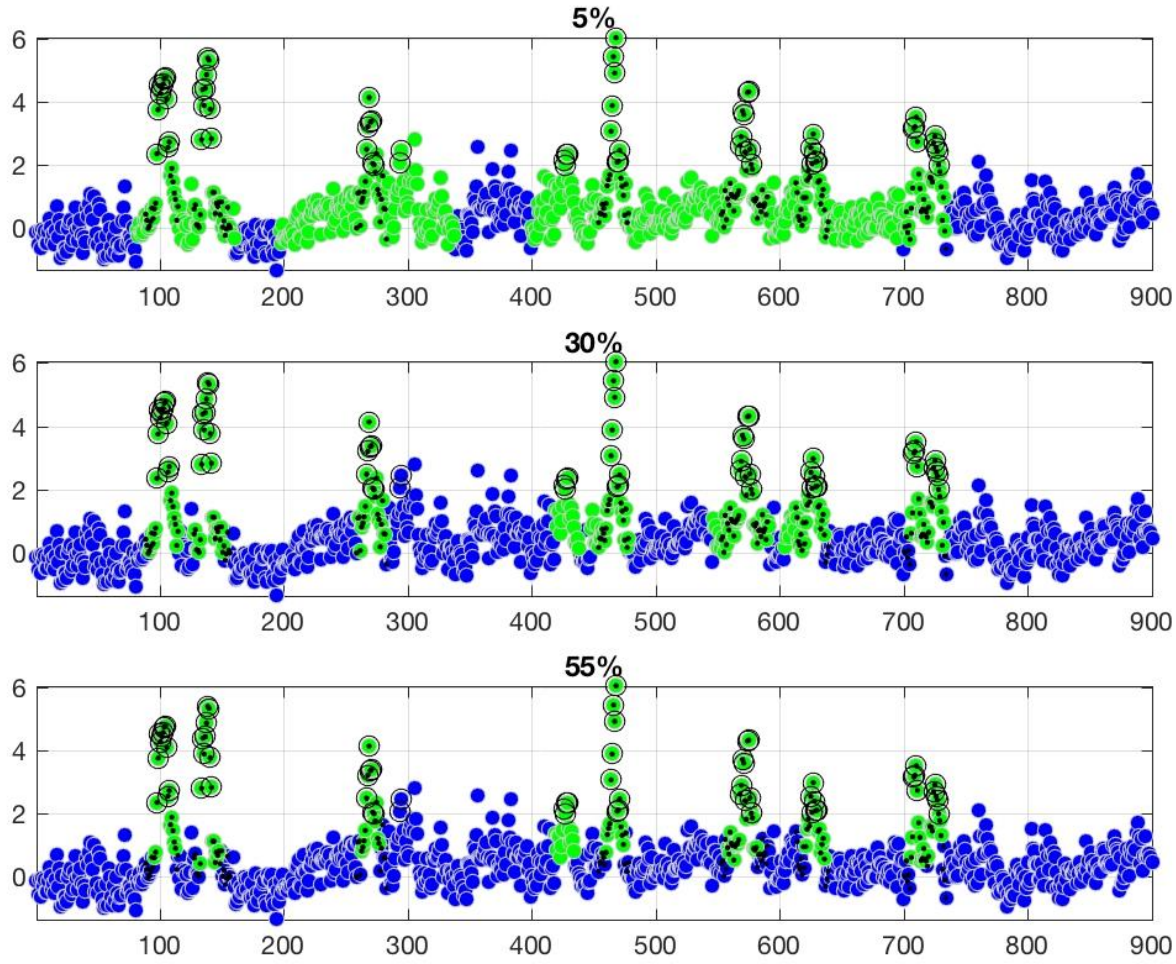

The figure above illustrates how the peak picking algorithm changes as a function of changing gpeak threshold. As seen by the green points indicating algorithm selected peaks, as the threshold is raised from 5% to 55%, the number and length of peaks is reduced. As before, the blue data indicates data inside the high threshold cluster in the Poincare map, the black dot indicates peaks identified by a human and the black circle indicates data inside the red polygonal region in the Poincare map. The threshold value used the find the peaks are indicated in the title of the plot.

The performance of the algorithm depends on the thresholds used to find the clusters in the Poincare map and the peak threshold. A training data set was created where a human identified peaks by hand for a total of 200 randomly selected traces. The peak detection algorithm processed the truth dataset and performance metrics were found, specifically, the ROC curve (FPR: 0.06, TPR 0.66), the Pierce Skill Score, the R-squared (linearity) for the amplitude of the peaks, and the number of true peaks found. Plots were generated for all the performance statistics as a function of the clustering and peak thresholds and threshold values were selected given the performance statistics.

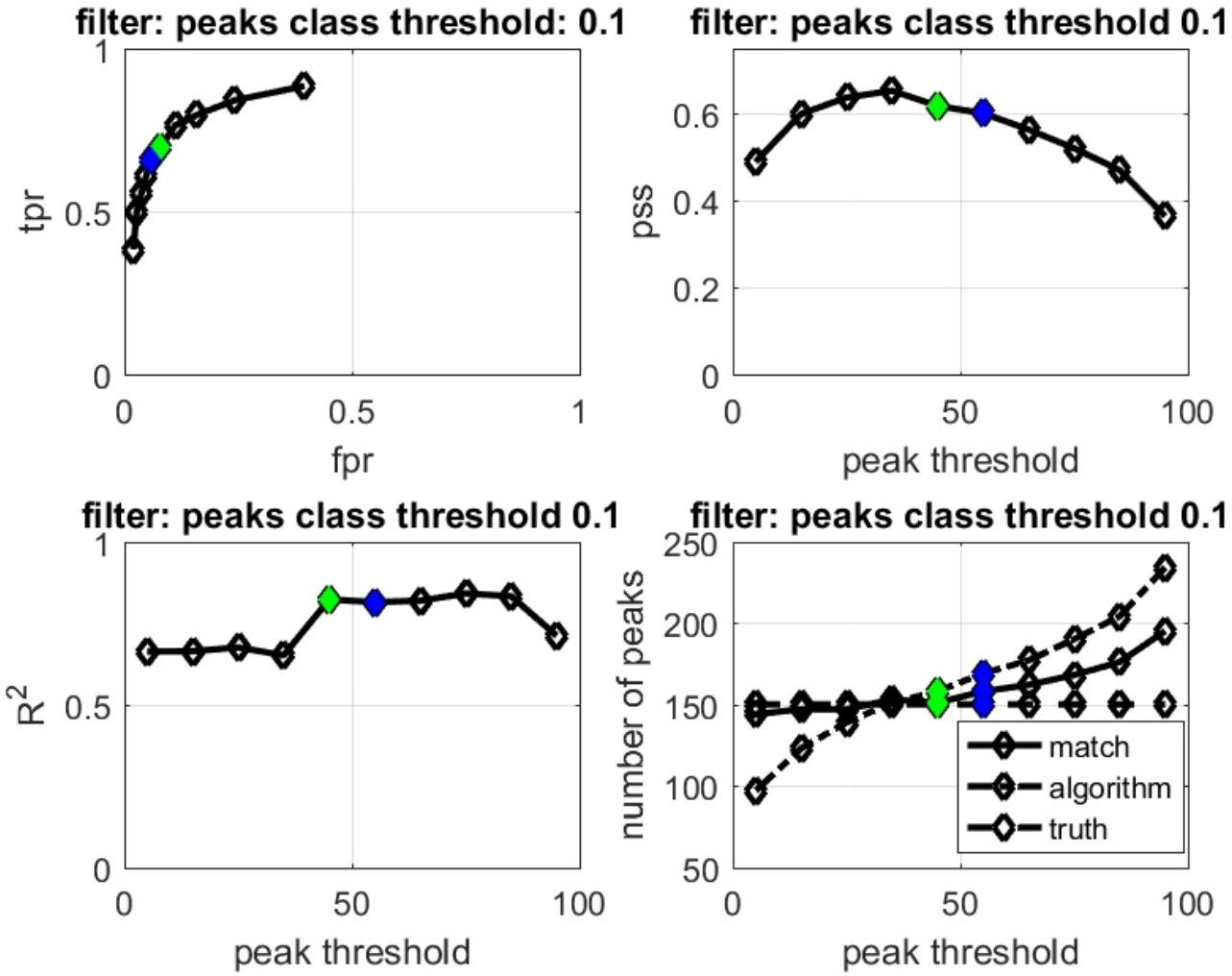

The figure above shows the ROC curve (upper left hand corner), the Pierce Skill Score (upper right hand corner), the R-squared of the algorithm peak amplitude and the truth peak amplitude (lower left hand corner) and the number of peaks found. The multiple curves for the number of peaks indicate the number of peaks that match the truth (solid line), the number of peaks found by the algorithm (dot-dash line) and the true number of peaks (dashed line) All statistics are plotted as a function of the peak threshold and the cluster threshold is indicated in the titles of the figures (0.1). The blue diamond indicates the peak threshold used for the results in the paper and the green diamond indicates an alternative threshold parameter.

The following figure shows scatter plots of the duration and amplitude of the peaks of the algorithm versus the truth data. Two threshold values are considered, 55% (blue) and 45% (green), which correspond to the blue and green diamonds in the plots for the ROC curve, Pierce Skill Score, R-square of the amplitude and the number of peaks. Heuristically, the performance of the algorithm is comparable for both parameter settings. The best fit to the data is shown in the corresponding color and the R-square value associated with the fit is given in the title.

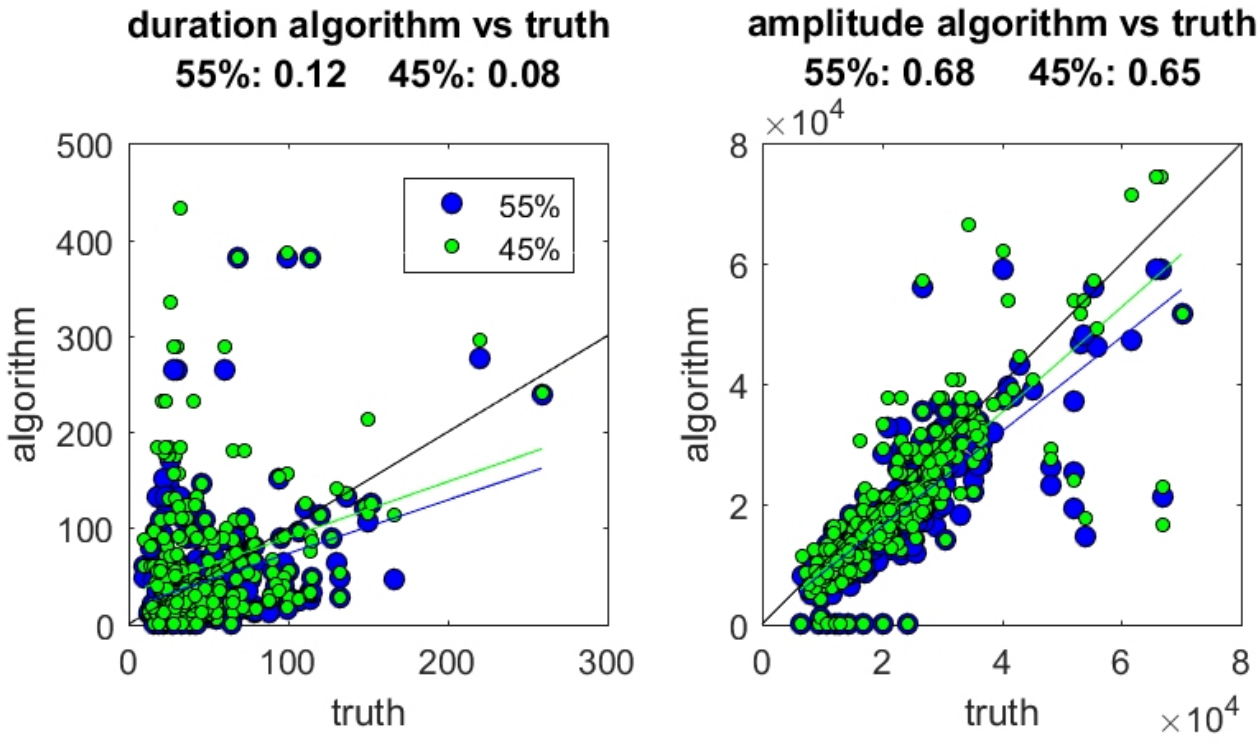

Genes used in this study:

Constitutive plasmid sequence with PROPS:

aactgatcttcagcatcttttactttcaccagcgtttctgggtgagcaaaaacaggaaggcaaaatgccgcaaaaaagggaataagggcgacacggaaat
gttgaatactcatactcttccttttcaatattattgaagcatttatcagggttattgtctcatgagcggatacatatttgaatgtatttagaaaaataaacaaatagg
ggttccgcgcacatttccccgaaaagtgccacctgacgtctaagaaaccattattatcatgacattaacctataaaaataggcgtatcacgaggcagaattt
cagataaaaaaaatccttagctttcgctaaggatgatttctggaattcgcggccgcatctagagttgacggctagctcagtcctaggtacagtgctagcaT
TAACTTTAAGAAGGAGATATACATACCCATGGGTAAATTATTACTGATATTAGGTAGTGTTA
TTGCACTTCCTACATTTGCTGCAGGTGGTGGTGACCTTGATGCTAGTGATTACACTGGTGTTT
CTTTTTGGTTAGTTACTGCTGCTTTATTAGCATCTACTGTATTTTTCTTTGTTGAAAGAGATAG
AGTTTCTGCAAAATGGAAAACATCATTAACTGTATCTGGTCTTGTTACTGGTATTGCTTTCTG
GCATTACATGTACATGAGAGGGGTATGGATTGAAACTGGTGATTCGCCAACTGTATTTAGAT
ACATTAATTGGTTACTAACAGTTCCTCTATTAATATGTGAATTCTACTTAATTCTTGCTGCTG
CAACTAATGTTGCTGGATCATTATTTAAGAAATTACTAGTTGGTTCTCTTGTTATGCTTGTGT
TTGGTTACATGGGTGAAGCAGGAATCATGGCTGCATGGCCTGCATTCATTATTGGGTGTTTA
GCTTGGGTATACATGATTTATGAATTATGGGCTGGAGAAGGAAAATCTGCATGTAATACTGC
AAGTCCTGCTGTGCAATCAGCTTACAACACAATGATGTATATTATCATCTTTGGTTGGGCGAT
TTATCCTGTAGGTTATTTCACAGGTTACCTGATGGGTGACGGTGGATCAGCTCTTAACTTAAA
CCTTATCTATAACCTTGCTGACTTTGTTAACAAGATTCTATTTGGTTTAATTATATGGAATGTT
GCTGTTAAAGAATCTTCTAATGCTCACCATCACCATCACCATTGAGTTTAAACGGTCTCCAGC
TTGGCTGTTTTGGCGGATGAGAGAAGATTTTCAGCCTGATACAGATTAAATCAGAACGCAGA
AGCGGTCTGATAAAACAGAATTTGCCTGGCGGCAGTAGCGCGGTGGTCCCACCTGACCCCAT
GCCGAACTCAGAAGTGAAACGCCGTAGCGCCGATGGTAGTGTGGGGTCTCCCCATGCGAGA
GTAGGGAACTGCCAGGCATCAAATAAAACGAAAGGCTCAGTCGAAAGACTGGGCCTTggcttcc
tcgctcactgactcgctgcgctcggtcgttcggctgcggcgagcggtatcagctcactcaaaggcggtaatacggttatccacagaatcaggggataac
gcaggaaagaacatgtgagcaaaaggccagcaaaaggccaggaaccgtaaaaaggccgcgttgctggcgtttttccataggctccgccccctgacg
agcatcacaaaaatcgacgctcaagtcagaggtggcgaaacccgacaggactataaagataccaggcgtttcccctggaagctccctcgtgcgctctc
ctgttccgaccctgccgcttaccggatacctgtccgcctttctcccttcgggaagcgtggcgctttctcatagctcacgctgtaggtatctcagttcggtgtag
gtcgttcgctccaagctgggctgtgtgcacgaacccccgttcagcccgaccgctgcgccttatccggtaactatcgtcttgagtccaacccggtaagac
acgacttatcgccactggcagcagccactggtaacaggattagcagagcgaggtatgtaggcggtgctacagagttcttgaagtggtggcctaactacg
gctacactagaaggacagtatttggtatctgcgctctgctgaagccagttaccttcggaaaaagagttggtagctcttgatccggcaaacaaaccaccgct
ggtagcggtggttttttgtttgcaagcagcagattacgcgcagaaaaaaaggatctcaagaagatcctttgatcttttctacggggtctgacgctcagtgga
acgaaaactcacgttaagggattttggtcatgagattatcaaaaaggatcttcacctagatccttttaaattaaaaatgaagttttaaatcaatctaaagtatatat
gagtaaacttggtctgacagttaccaatgcttaatcagtgaggcacctatctcagcgatctgtctatttcgttcatccatagttgcctgactccccgtcgtgtag
ataactacgatacgggagggcttaccatctggccccagtgctgcaatgataccgcgagacccacgctcaccggctccagatttatcagcaataaaccag
ccagccggaagggccgagcgcagaagtggtcctgcaactttatccgcctccatccagtctattaattgttgccgggaagctagagtaagtagttcgccag
ttaatagtttgcgcaacgttgttgccattgctacaggcatcgtggtgtcacgctcgtcgtttggtatggcttcattcagctccggttcccaacgatcaaggcga
gttacatgatcccccatgttgtgcaaaaaagcggttagctccttcggtcctccgatcgttgtcagaagtaagttggccgcagtgttatcactcatggttatggc
agcactgcataattctcttactgtcatgccatccgtaagatgcttttctgtgactggtgagtactcaaccaagtcattctgagaatagtgtatgcggcgaccga
gttgctcttgcccggcgtcaatacgggataataccgcgccacatagcagaactttaaaagtgctcatcattggaaaacgttcttcggggcgaaaactctca
aggatcttaccgctgttgagatccagttcgatgtaacccactcgtgcaccc

CaPR sequence used in constitutive plasmid (PROPS + GCaMP6f):

ATGGGTAAATTATTACTGATATTAGGTAGTGTTATTGCACTTCCTACATTTGCTGCAGGTGGT
GGTGACCTTGATGCTAGTGATTACACTGGTGTTTCTTTTTGGTTAGTTACTGCTGCTTTATTAG
CATCTACTGTATTTTTCTTTGTTGAAAGAGATAGAGTTTCTGCAAAATGGAAAACATCATTAA
CTGTATCTGGTCTTGTTACTGGTATTGCTTTCTGGCATTACATGTACATGAGAGGGGTATGGA
TTGAAACTGGTGATTCGCCAACTGTATTTAGATACATTAATTGGTTACTAACAGTTCCTCTAT

TAATATGTGAATTCTACTTAATTCTTGCTGCTGCAACTAATGTTGCTGGATCATTATTTAAGA
AATTACTAGTTGGTTCTCTTGTTATGCTTGTGTTTGGTTACATGGGTGAAGCAGGAATCATGG
CTGCATGGCCTGCATTCATTATTGGGTGTTTAGCTTGGGTATACATGATTTATGAATTATGGG
CTGGAGAAGGAAAATCTGCATGTAATACTGCAAGTCCTGCTGTGCAATCAGCTTACAACACA
ATGATGTATATTATCATCTTTGGTTGGGCGATTTATCCTGTAGGTTATTTCACAGGTTACCTG
ATGGGTGACGGTGGATCAGCTCTTAACTTAAACCTTATCTATAACCTTGCTGACTTTGTTAAC
AAGATTCTATTTGGTTTAATTATATGGAATGTTGCTGTTAAAGAATCTTCTAATGCTATGGGT
TCTCATCATCATCATCATCATGGTATGGCTAGCATGACTGGTGGACAGCAAATGGGTCGGGA
TCTGTACGACGATGACGATAAGGATCTCGCCACCATGGTCGACTCATCACGTCGTAAGTGGA
ATAAGACAGGTCACGCAGTCAGAGCTATAGGTCGGCTGAGCTCACTCGAGAACGTCTATATC
AAGGCCGACAAGCAGAAGAACGGCATCAAGGCGAACTTCAAGATCCGCCACAACATCGAG
GACGGCGGCGTGCAGCTCGCCTACCACTACCAGCAGAACACCCCCATCGGCGACGGCCCCG
TGCTGCTGCCCGACAACCACTACCTGAGCGTGCAGTCCAAACTTTCGAAAGACCCCAACGAG
AAGCGCGATCACATGGTCCTGCTGGAGTTCGTGACCGCCGCCGGGATCACTCTCGGCATGGA
CGAGCTGTACAAGGGCGGTACCGGAGGGAGCATGGTGAGCAAGGGCGAGGAGCTGTTCACC
GGGGTGGTGCCCATCCTGGTCGAGCTGGACGGCGACGTAAACGGCCACAAGTTCAGCGTGT
CCGGCGAGGGTGAGGGCGATGCCACCTACGGCAAGCTGACCCTGAAGTTCATCTGCACCAC
CGGCAAGCTGCCCGTGCCCTGGCCCACCCTCGTGACCACCCTGACCTACGGCGTGCAGTGCT
TCAGCCGCTACCCCGACCACATGAAGCAGCACGACTTCTTCAAGTCCGCCATGCCCGAAGGC
TACATCCAGGAGCGCACCATCTTCTTCAAGGACGACGGCAACTACAAGACCCGCGCCGAGG
TGAAGTTCGAGGGCGACACCCTGGTGAACCGCATCGAGCTGAAGGGCATCGACTTCAAGGA
GGACGGCAACATCCTGGGGCACAAGCTGGAGTACAACCTGCCGGACCAACTGACTGAAGAG
CAGATCGCAGAATTTAAAGAGGAATTCTCCCTATTTGACAAGGACGGGGATGGGACAATAA
CAACCAAGGAGCTGGGGACGGTGATGCGGTCTCTGGGGCAGAACCCCACAGAAGCAGAGCT
GCAGGACATGATCAATGAAGTAGATGCCGACGGTGACGGCACAATCGACTTCCCTGAGTTC
CTGACAATGATGGCAAGAAAAATGAAATACAGGGACACGGAAGAAGAAATTAGAGAAGCG
TTCGGTGTGTTTGATAAGGATGGCAATGGCTACATCAGTGCAGCAGAGCTTCGCCACGTGAT
GACAAACCTTGGAGAGAAGTTAACAGATGAAGAGGTTGATGAAATGATCAGGGAAGCAGA
CATCGATGGGGATGGTCAGGTAAACTACGAAGAGTTTGTACAAATGATGACAGCGAAGTAA

GCaMP6f + linker + mRuby3 sequence used in constitutive plasmid:

ATGGGTTCTCATCATCATCATCATCATGGTATGGCTAGCATGACTGGTGGACAGCAAATGGG
TCGGGATCTGTACGACGATGACGATAAGGATCTCGCCACCATGGTCGACTCATCACGTCGTA
AGTGGAATAAGACAGGTCACGCAGTCAGAGCTATAGGTCGGCTGAGCTCACTCGAGAACGT
CTATATCAAGGCCGACAAGCAGAAGAACGGCATCAAGGCGAACTTCAAGATCCGCCACAAC
ATCGAGGACGGCGGCGTGCAGCTCGCCTACCACTACCAGCAGAACACCCCCATCGGCGACG
GCCCCGTGCTGCTGCCCGACAACCACTACCTGAGCGTGCAGTCCAAACTTTCGAAAGACCCC
AACGAGAAGCGCGATCACATGGTCCTGCTGGAGTTCGTGACCGCCGCCGGGATCACTCTCGG
CATGGACGAGCTGTACAAGGGCGGTACCGGAGGGAGCATGGTGAGCAAGGGCGAGGAGCT
GTTCACCGGGGTGGTGCCCATCCTGGTCGAGCTGGACGGCGACGTAAACGGCCACAAGTTC
AGCGTGTCCGGCGAGGGTGAGGGCGATGCCACCTACGGCAAGCTGACCCTGAAGTTCATCT
GCACCACCGGCAAGCTGCCCGTGCCCTGGCCCACCCTCGTGACCACCCTGACCTACGGCGTG
CAGTGCTTCAGCCGCTACCCCGACCACATGAAGCAGCACGACTTCTTCAAGTCCGCCATGCC
CGAAGGCTACATCCAGGAGCGCACCATCTTCTTCAAGGACGACGGCAACTACAAGACCCGC
GCCGAGGTGAAGTTCGAGGGCGACACCCTGGTGAACCGCATCGAGCTGAAGGGCATCGACT
TCAAGGAGGACGGCAACATCCTGGGGCACAAGCTGGAGTACAACCTGCCGGACCAACTGAC
TGAAGAGCAGATCGCAGAATTTAAAGAGGAATTCTCCCTATTTGACAAGGACGGGGATGGG
ACAATAACAACCAAGGAGCTGGGGACGGTGATGCGGTCTCTGGGGCAGAACCCCACAGAAG
CAGAGCTGCAGGACATGATCAATGAAGTAGATGCCGACGGTGACGGCACAATCGACTTCCC
TGAGTTCCTGACAATGATGGCAAGAAAAATGAAATACAGGGACACGGAAGAAGAAATTAG

AGAAGCGTTCGGTGTGTTTGATAAGGATGGCAATGGCTACATCAGTGCAGCAGAGCTTCGCC
ACGTGATGACAAACCTTGGAGAGAAGTTAACAGATGAAGAGGTTGATGAAATGATCAGGGA
AGCAGACATCGATGGGGATGGTCAGGTAAACTACGAAGAGTTTGTACAAATGATGACAGCG
AAGggtGGATCCggtggtagcggtggtagcggtGGATCCATGGTGTCTAAGGGCGAAGAGCTGATCAAGG
AAAATATGCGTATGAAGGTGGTCATGGAAGGTTCGGTCAACGGCCACCAATTCAAATGCAC
AGGTGAAGGAGAAGGCAGACCGTACGAGGGAACTCAAACCATGAGGATCAAAGTCATCGA
GGGAGGACCCCTGCCATTTGCCTTTGACATTCTTGCCACGTCGTTCATGTATGGCAGCCGTAC
TTTTATCAAGTACCCGGCCGACATCCCTGATTTCTTTAAACAGTCCTTTCCTGAGGGTTTTAC
TTGGGAAAGAGTTACGAGATACGAAGATGGTGGAGTCGTCACCGTCACGCAGGACACCAGC
CTTGAGGATGGCGAGCTCGTCTACAACGTCAAGGTCAGAGGGGTAAACTTTCCCTCCAATGG
TCCCGTGATGCAGAAGAAGACCAAGGGTTGGGAGCCTAATACAGAGATGATGTATCCAGCA
GATGGTGGTCTGAGAGGATACACTGACATCGCACTGAAAGTTGATGGTGGTGGCCATCTGCA
CTGCAACTTCGTGACAACTTACAGGTCAAAAAAGACCGTCGGGAACATCAAGATGCCCGGT
GTCCATGCCGTTGATCACCGCCTGGAAAGGATCGAGGAGAGTGACAATGAAACCTACGTAG
TGCAACGCGAAGTGGCAGTTGCCAAATACAGCAACCTTGGTGGTGGCATGGACGAGCTGTA
CAAG

Supplementary References:

1. Taniguchi Y, et al. (2010) Quantifying E. coli proteome and transcriptome with single-molecule sensitivity in single cells. *Science (80-)* 329(5991):533–8.
2. Baba T, et al. (2006) Construction of Escherichia coli K-12 in-frame, single-gene knockout mutants: the Keio collection. *Mol Syst Biol* 2:2006.0008.
3. Barnett L, Seth AK (2014) The MVGC multivariate Granger causality toolbox: A new approach to Granger-causal inference. *J Neurosci Methods* 223:50–68.